

## Hybrid Ti-ceramic bionanomaterials for dental engineering

M. Jurczyk<sup>1</sup> K. Jurczyk<sup>2</sup> K. Niespodziana<sup>1</sup> & A. Miklaszewski<sup>1</sup>

<sup>1</sup> *Poznan University of Technology, Inst. Mat. Sc. Eng. Poznan, Poland*

<sup>2</sup> *Medical University, Dep. Conserv. Dent. Period., Poznan, Poland*

**INTRODUCTION:** In the last decade a great interest has been observed in the field of nanoscale biomaterials [1]. One of the methods that allows the change of properties of Ti alloys is to produce nanocomposite, which will exhibit the favorable mechanical properties of titanium and excellent biocompatibility and bioactivity of ceramics [2]. In this work, the titanium-ceramic nanocomposites with 3 and 10 wt% of hydroxyapatite (HA), 45S5 Bioglass, SiO<sub>2</sub> or Al<sub>2</sub>O<sub>3</sub> were prepared.

**METHODS:** The titanium-ceramic nano-composites were produced by the combination of mechanical alloying and powder metallurgical process [2]. The synthesized bulk samples were examined by XRD and TEM. The crystallite sizes were estimated from the half-width of lines using the Scherrer equation. The effect of the different content of ceramic powders on mechanical properties of titanium was assessed by Vickers' microhardness measurements. Corrosion test was performed in Ringer's solution at T=37 ± 1°C. The cytotoxicity tests were performed in static and dynamic conditions [3].

**RESULTS:** The Ti-ceramic mixtures milled for more than 20 h have transformed completely to an amorphous phase. Formation of the nanocrystalline Ti-ceramic composites was achieved by annealing of the amorphous material [2]. According to the Scherrer method of XRD profiles, the average crystallite size of titanium-ceramic nanocomposites mechanically alloyed and heat treated was about 40 nm. The Vickers' microhardness of Ti-ceramic is higher than that of pure microcrystalline titanium. Additionally, Ti-based nanocomposites have good corrosion resistance. The relative viability of the cells (RVC) decreases when fraction increases. It is important to note that the RVC of nanoscale Ti-10 wt% SiO<sub>2</sub> is higher in comparison with microcrystalline titanium.

**DISCUSSION & CONCLUSIONS:** The combination of mechanical alloying and powder metallurgy process succeeded in the production of titanium-ceramic nanocomposites. XRD analysis of all heat treated titanium-ceramic nanocomposites showed the presence of α-Ti type structure (hexagonal-type structure) with nanograins of ceramic phases. The results show an enhancement of hardness due to the nanoscale structures in consolidated materials. The Vickers' micro-hardness of the sintered nanocomposites exhibit

various distribution corresponding to constitutional change and increases with the rise of ceramic contents. The Vickers' microhardness strongly increases for Ti-10 wt% HA nanocomposites (1500 HV0.2) particularly and is six times higher than of pure microcrystalline Ti

metal (250 HV0.2). Vickers' microhardness of other sintered nano-composites is almost two or three times higher than that of pure microcrystalline Ti metal. The ceramics doped to titanium had a positive effect on corrosion resistance of titanium in Ringer's solutions. Titanium composite with 3 wt% of HA had the highest corrosion resistance ( $I_c = 9.06 \cdot 10^{-8}$  A/cm<sup>2</sup>,  $E_c = -0.34$  V from among sintered nanocomposites. As it can be observed, other nanocomposites have better corrosion resistance in comparison with microcrystalline titanium ( $1.31 \cdot 10^{-5}$  A/cm<sup>2</sup>). Application of Ti-ceramic nanocomposites focused also our attention on the biocompatibility of synthesized bulk materials. After 1<sup>st</sup> day of incubation cells show good adhesion to the surface of studied samples in the form of filopodia. After 5 days of in-cubation, the typical monolayer was observed. Earlier, it has been demonstrated that metal (Ti, Ti6Al4V) surfaces utilizing submicron to nanometer particles, due to higher amounts of particle boundaries at their surfaces, promoted the adhesion of osteoblasts compared to metals composed of respective micron particles [3]. This research will be the gateway for traditional industry to nanotechnology and knowledge-based materials, with positive effects on the environmental and health issues. Nanoscience and nanotechnology can provide tremendous new possibilities never experienced before in dental practice.

**REFERENCES:** <sup>1</sup> H.N. Liu, T.J. Webster (2007) *Biomaterials* 28: 354-369. <sup>2</sup> K. Niespodziana, K. Jurczyk, M. Jurczyk (2009) *Solid State Phenom.* 151: 217-221. <sup>3</sup> A. Yamamoto, Y. Kohyama, D. Kuroda, T. Hanawa, (2004) *Mater. Sci. Eng. C* 24: 737-743.

**ACKNOWLEDGEMENTS:** Polish Ministry of Science and Higher Education Contract No.N507 071 32/2092

## Deposition and Properties of Hydroxyapatite on Flat and Porous Ti

J. Jakubowicz

*Institute of Materials Science and Engineering, Poznan University of Technology,  
M. Skłodowska-Curie 5 Sq., 60-965 Poznan, Poland*

**INTRODUCTION:** Formation of porous Ti layer during electrochemical etching in  $\text{H}_3\text{PO}_4 + \text{NH}_4\text{F}$ , subsequent deposition of hydroxyapatite (Fig. 1) and corrosion behavior of the materials was described (Tab. 1).

**METHODS:** The used source of Ca and P were two types of electrolytes:

- (i) 0.1M HCl + 0.005M HA (particles),
- (ii) 0.042M  $\text{Ca}(\text{NO}_3)_2 + 0.025 (\text{NH}_4)_2\text{HPO}_4 + 0.1\text{M HCl}$ .

**RESULTS:** Anodic etching results in surface roughening with pits with diameter in the range of 7-12  $\mu\text{m}$  [1]. The subsequent cathodic electrochemical treatment, results in hydroxyapatite (HA) deposition.

The formed HA layer has lamellas structure (Fig. 1). The deposited calcium-phosphate layer is useful for the osseointegration and presents excellent corrosion resistance in simulated body fluids (Tab. 1). The corrosion current  $I_c$  for pure Ti, porous Ti and porous Ti with Ca-P layer is:  $3.9 \cdot 10^{-8} \text{ A}\cdot\text{cm}^{-2}$ ,  $2.52 \cdot 10^{-8} \text{ A}\cdot\text{cm}^{-2}$  and  $1.07 \cdot 10^{-8} \text{ A}\cdot\text{cm}^{-2}$ , respectively.

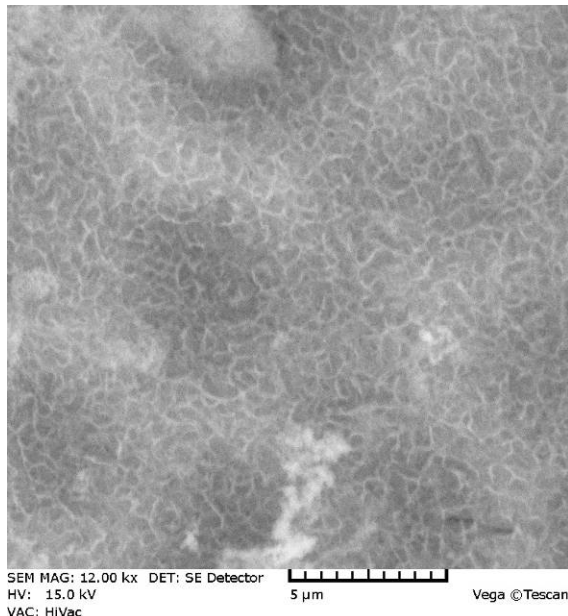


Fig. 1: Hydroxyapatite deposited from HA + HCl electrolyte on porous Ti (pores with deposited HA are still visible as darker spots).

Table 1. Corrosion current  $I_c$  and corrosion potential  $E_c$  for the flat not etched Ti, porous

*electrochemically etched Ti, and Ti both flat and porous, with deposited calcium-phosphate.*

Sample	$I_c$ ( $\text{A}/\text{cm}^2$ )	$E_c$ (V)
Ti – not etched	$3.90 \cdot 10^{-8}$	-0.46
Ti – not etched with deposited Ca-P using electrolyte: (i)	$1.57 \cdot 10^{-8}$	-0.66
Ti – not etched with deposited Ca-P using electrolyte: (ii)	$3.92 \cdot 10^{-8}$	-0.77
Ti – etched	$2.52 \cdot 10^{-8}$	-0.90
Ti – etched with deposited Ca-P using electrolyte: (i)	$1.47 \cdot 10^{-8}$	-0.86
Ti – etched with deposited Ca-P using electrolyte: (ii)	$1.07 \cdot 10^{-8}$	-0.25

**DISCUSSION & CONCLUSIONS:** It was found, that anodization and subsequent calcium-phosphate deposition, results in better corrosion resistance of the samples, with comparison to sample without these treatments, which is extremely important for hard tissue implant application.

**REFERENCES:** <sup>1</sup> J. Jakubowicz (2008) *Electrochem. Commun.* **10**:735-739.

**ACKNOWLEDGEMENTS:** The financial support of the Polish Ministry of Education and Science under the contract No N N507 277536 is gratefully acknowledged.

## Microfluidic devices for biological applications

S Potgieter<sup>1</sup>, K Land<sup>1</sup>, L Kotze<sup>1</sup> & R Sparrow<sup>2</sup>

<sup>1</sup>CSIR Materials Science and Manufacturing, South Africa, <sup>2</sup>CSIR Biosciences, South Africa

**INTRODUCTION:** Microfluidics is a multi-disciplinary field that deals with the behaviour, control and manipulation of fluids constrained to sub-millilitre volumes. It is proving to be a useful tool for biological studies, affording advantages such as reduced cost, faster reaction times and process-specific designs. A microfluidic system typically consists of a series of channels with components like pumps, valves and actuators to control the flow of fluids<sup>1</sup>.

These systems are employed in what is known as “lab-on-chip” devices, where a chip is manufactured to perform a specific chemical reaction or diagnostic test. The chip contains beakers, test tubes, mixers, and particle separators, all on micro scale. A malaria test is transformed from a few-hour, multi-person, resource intensive process to a disposable, easy-to-use process where the only training necessary is the ability to place a drop of blood on a sensor and interpret an intuitive result<sup>2</sup>.

A micro-manufacturing facility is being established at the CSIR, Material Science and Manufacturing. The focus is on microfluidics, utilising a soft lithography process. Various components of microfluidic devices have been manufactured and successfully tested. These include valves and mixers. Components that are currently being investigated include emulsion generation devices, particle sorting devices, sensors for measuring flow rate and concentration and variable reaction time circuits.

**METHODS:** One of the applications being worked on is a microfluidic emulsification device (MES). It will be used to produce monodisperse Spheryzyme particles, an enzyme manufacturing process patented by the CSIR. The MES will allow scale-up of the manufacturing process and will significantly reduce the size distribution of the enzymes. Possible issues which will need to be considered include damage or denaturing of the enzymes during the production process.

Another project deals with designing a microfluidic device to assemble biological nano-machines that convert light energy into mechanical movement. Due to their small size, handling the

components and fabricating the nano-machines is a challenging task. A further complication is that the components are required in specified numbers and an established sequence. Self-assembly combined with microfluidics is a promising way to overcome these difficulties.

**RESULTS:** Proof-of-concept studies have been undertaken on generating emulsions using microfluidic channels. Figure 1 shows an example. The figure shows an emulsion of water and oil. The next steps are to include surfactants, crosslinkers and enzymes and verify the results.

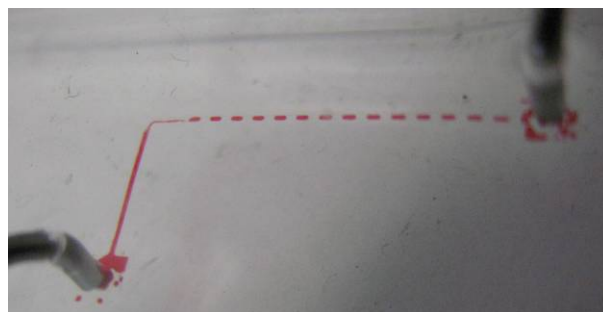


Fig. 1: Emulsion generation using a microfluidic channel.

### DISCUSSION & CONCLUSIONS:

Microfluidics provides a useful platform for drug delivery, chemical synthesis and medical diagnostics. All indications are that it will play an increasing role in our lives in future – it is believed that microfluidics will solve integration problems in biology and chemistry in the same way that integrated circuits did for microelectronics.

This technology is of critical importance to South Africa, and has resulted in the current effort to introduce the technology and develop the knowledge required to make an impact in the South African economy and health sectors. Furthermore, it is aligned to the national R+D strategy and the Department of Science and Technology’s 10 year innovation plan.

**REFERENCES:** <sup>1</sup> G.M. Whitesides (2006) *Nature* **442**:368-373. <sup>2</sup> C.D. Chin, V. Linder, S.K.Sia (2007) *Lab Chip* **7**:41-57.

## Electrospun Chitosan Nanofibre Membranes for Antimicrobial Application: Role of Electrospinning Processing Parameters

Valencia Jacobs<sup>1, 2</sup> Asis Patanaik<sup>1</sup> & Rajesh D. Anandjiwala<sup>1, 2</sup>

<sup>1</sup>CSIR Materials Science and Manufacturing, Polymers and Composites Competence Area, P.O. Box 1124, Port Elizabeth 6000, South Africa. <sup>2</sup>Department of Textile Science, Faculty of Science, Nelson Mandela Metropolitan University, P.O. Box 77000, Port Elizabeth 6031, South Africa

**INTRODUCTION:** Electrospinning is a straightforward and versatile technique for fabrication of nanofibres from a variety of polymer solutions.<sup>1</sup> Nanofibers with high surface area to volume ratio, high porosity and small fiber diameter make them ideal materials for biomedical applications such as wound dressing.<sup>2</sup> In this paper, we report investigation on the effects of governing parameters on the formation of chitosan nanofibre membranes. These membranes were subjected to various cell cultures for antibacterial properties.

**METHODS:** Various concentrations of chitosan-based solutions in the range of 2-5% were prepared in acidic solutions. The polymeric solutions were electrospun under various processing electrospinning parameters to form nanofibre membranes. The electrospinning setup utilized in this study consists of a Pasteur pipette, an electrically grounded metal screen. A high voltage power supply was used to produce voltages ranging from 0 - 30kV and a distance of 10 to 20 cm was maintained between the nozzle and the collector screen.

Antibacterial properties of the electrospun nanofibres was determined by subjecting the membranes into a well that has been made in the agar plate containing *E.Coli* or *S.Aureus*, and then incubated at 37°C.

The fiber diameter and structural morphology of electrospun chitosan fibers were determined using FEI Quanta 200 Scanning Electron Microscope (SEM).

**RESULTS:** Electrospinning of pure chitosan solutions from weak acids has been a challenge as previously mentioned by previous authors.<sup>3</sup> Thus, the combination of weak acids and volatile solvents increased the capacity of nanofiber formation. The form of electrospun membranes was also encouraged by blending chitosan with PEO. As the chitosan concentration (PEO-chitosan) increases, the bead formation decreases.

Neither *E.Coli* nor *S.Aureus* growth was inhibited by PEO-chitosan nanofiber membranes.

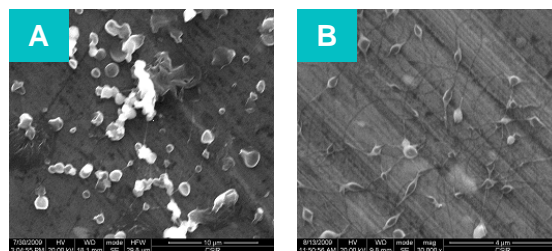


Fig. 1: SEM images showing the effect of chitosan concentration on the bead formation of electrospun nanofiber membranes: A) PEO nanofibers. B) PEO-chitosan nanofibers.

Table 1. Cell growth inhibition of electrospun nanofibers.

Nanofibres	Organism Tested	
	<i>E.Coli</i> (37°C)	<i>S.Aureus</i> (37°C)
PEO	0	0
PEO-Chitosan	0	0

**DISCUSSION & CONCLUSIONS:** A blended chitosan nanofibers with electrospinnable PEO polymer encourages the formation of electrospun membranes. Mixture of weak acidic solution with volatile solvent improves the capacity of electrospun nanofibers. Various concentration ratios of PEO-Chitosan nanofiber membranes exhibited no biotoxicity.

**REFERENCES:** <sup>1</sup> D.H. Reneker and I. Chun (1996) *Nanotechnol* 7:216-23. <sup>2</sup> S. Hirano (1999) *Polym Int* 48:732-34. <sup>3</sup> C.K.S. Pillai and C.P. Sharma (2009) *Trends Biomater Artif Organs* 22:175-97.

## Glycosaminoglycans and lipids in vascular calcification: new insights into mineralogenesis from NMR spectroscopy

M.J.Duer<sup>1</sup> M.S.Ironside<sup>1</sup> D.G. Reid<sup>1</sup> M. Schoppet<sup>2</sup> & C.M.Shanahan<sup>3</sup>

<sup>1</sup>Dept. Chemistry, U. Cambridge, Cambridge, UK. <sup>2</sup>Dept. of Internal Medicine and Cardiology, Philipps-University, Marburg, Germany. <sup>3</sup>Cardiovascular Division, Kings College London, UK

**INTRODUCTION:** Vascular calcification is common in atherosclerosis, and its extent and severity is associated with cardiovascular mortality. Hydroxyapatitic calcium phosphate particles can be pro-inflammatory, can affect the predisposition of plaques to rupture, and are particularly prevalent in diabetic and renal failure patients. We have recently shown that the cellular and molecular signalling similarities well documented between orthotopic bone formation and pathological (heterotopic) vascular calcification are recapitulated at the atomic level, with the predominant macromolecules forming the mineral interface with the organic matrix in both tissues being glycosaminoglycan (GAG) polysaccharides [1,2].



Fig.1: Extensively calcified atherosclerotic plaque from a patient with peripheral artery disease, with scale bar.

**METHODS:** Human calcified atherosclerotic vascular plaque specimen was obtained after surgical amputation of the lower limb. Mineral free of organic matrix material was produced by digestion over several weeks with caustic soda and bleach until no further changes were seen in the <sup>13</sup>C NMR of the mineral. NMR methodology is described in Ref. 1.

**RESULTS:** Figure 2 compares <sup>13</sup>C spectra from exhaustively digested calcified atherosclerotic plaque, and bone, mineral. The bone mineral is characterized by the almost complete absence of signal from organic material, the exception being the sharp peak at 30 ppm from fatty acid lipids. On the other hand the mineral from atherosclerotic plaque shows a rich spectrum of organic components, including signals ascribable to GAGs, cholesterol, glycerides and fatty acids.

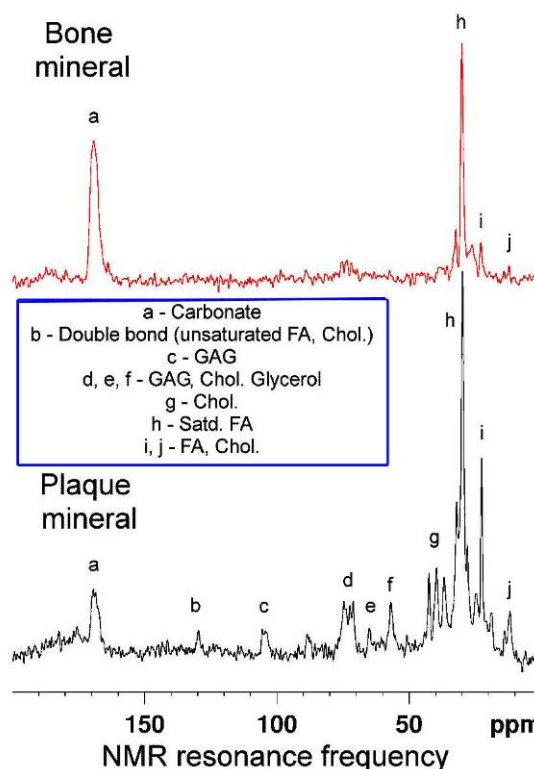


Fig. 2: <sup>13</sup>C NMR of pure biomineral from bone vs. plaque, showing entrapped organic components.

**DISCUSSION & CONCLUSIONS:** Finding any organic signal in pure bone and plaque mineral was very surprising. However, GAGs and lipids are prominent in most models of mineralization [3]. Is NMR showing a “fossil record” of the participating GAGs and vesicles, in which the “molecular machinery” of biomineralization has been arrested and entrapped at an early stage? Characterization of the molecules and intermolecular associations thus preserved will shed new light on pathological mineralization mechanisms and yield new insights for their control and treatment.

**REFERENCES:** <sup>1</sup>M.J.Duer et al. (2008) *Arterioscl. Thromb. Vasc. Biol.* **28**: 2030-4. <sup>2</sup>M.J.Duer et al. (2007) *Chem. Mater.* **19**:5055-7. <sup>3</sup>L.L.Demer, A.P.Sage, Y.Tintut *Arterioscl. Thromb. Vasc. Biol.* **28**: 1882-4.

**ACKNOWLEDGEMENTS:** UK BBSRC and EPSRC, British Heart Foundation.

## Liposomes as a drug delivery system in photodynamic therapy for colon cancer treatment

K Maduray<sup>1,2</sup> & AE Karsten<sup>1</sup>

<sup>1</sup> Biophotonics, NLC, CSIR, Pretoria. <sup>2</sup> Durban University of Technology, Durban, South Africa.

**INTRODUCTION:** Photodynamic therapy (PDT) uses a drug termed a photosensitizer (PS), light (laser) of an appropriate wavelength and molecular oxygen (tissue) to elicit cell death of cancer cells [1]. Liposome preparations are currently used as an effective drug delivery system or carrier in PDT. Liposome consists of an aqueous core and lipophilic space between the lipid bilayer. These properties make liposomes a powerful drug delivery system as it encapsulates both hydrophilic and hydrophobic drugs in high loading capacity [2].

The objective of this study was to evaluate the enhancement of PDT efficiency by using a liposome drug delivery system with different drug concentrations in contrast to treatment excluding the use of the drug delivery system on a colon cancer cell line.

**METHODS:** DLD-1 (colon cancer cell line) cells were seeded in 24-well cell culture plates and incubated for 24 hours, after which they were pretreated with different concentrations of the PS (zinc tetrasulfophthalocyanine/ZnTSPc) containing egg yolk lecithin (liposome drug delivery system). Control cells were pretreated with the same PS concentrations but without the liposome drug delivery system. The photosensitized cells were incubated for 2 hours before irradiation with a 672nm diode laser. The output power of the continuous wave laser was 33mW. A beam diameter of 1cm was used to deliver 4.5J/cm<sup>2</sup> in 107 seconds. Post-irradiated cells were incubated for 24 hours before cell death was measured using the Cell Titer-Blue™ Viability Assay from Promega Corporation.

### RESULTS:

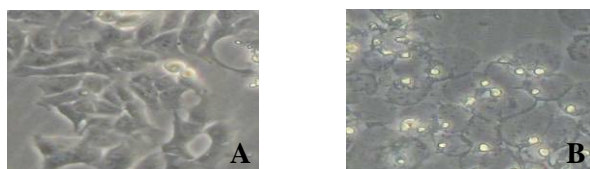


Fig. 1: The micrographs (32x) shows the cell morphology of DLD-1 cells untreated (A) and after liposomal – mediated PDT treatment (B).

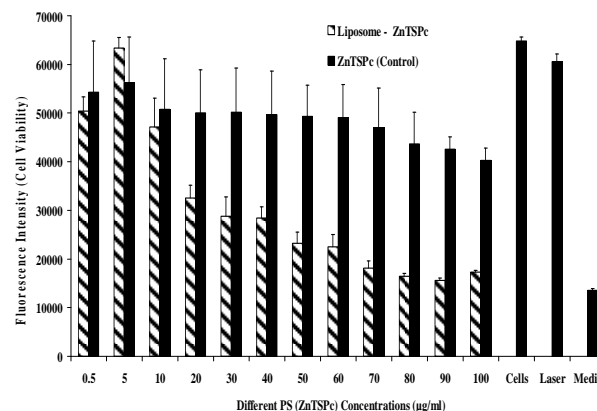


Fig. 2: The cell viability of DLD-1 cells photosensitized by liposome-mediated ZnTSPc and controls prior to light activation.

**DISCUSSION & CONCLUSIONS:** DLD-1 cells treated with liposome-mediated ZnTSPc were able to decrease cell viability more extensively than the control cells (Fig. 2). This showed that the efficiency of the photodynamic effect was enhanced with liposome-mediated PS prior to light activation. DLD-1 cells subjected to liposome-mediated PS manifested morphological changes indicating cell death via the secondary necrosis mechanism (Fig. 1). This indicates that the use of liposome drug delivery system is advantageous as it enables lower drug concentrations to be administered with enhanced PDT activity, thus reducing the side effects and causing less damage to healthy tissue. This concludes that the use of liposome as a drug delivery system can enhance PDT efficacy and safety by using lower concentrations of the PS (ZnTSPc) to destroy the cancer cells.

**REFERENCES:** <sup>1</sup> A.S.L. Derycke and P.A.M. De Witte (2004) *Advanced Drug Delivery Reviews* **56**: 17-30. <sup>2</sup> B. Chen, B.W. Pogue and T. Hasan (2005) *Expert Opinion Drug Delivery* **2**: 477-487.

**ACKNOWLEDGEMENTS:** This project is funded by CSIR, NLC, Biophotonics group. We would like to thank Dr Clement Penny (Senior Lecturer at the University of Witwatersrand, Oncology Division) for providing the DLD-1 cells (Colon cancer cell line) and Professor Tebello Nyokong (Rhodes University, Department of Chemistry) for the ZnTSPc.

## Biocompatibility of Dendrispheres

[S. Garny](#)<sup>1</sup> [I. Gerber](#)<sup>1</sup> & [J. Jordaan](#)<sup>1</sup>

<sup>1</sup> CSIR Biosciences, Synthetic Biology ERA, Molecular Biomaterials Research Group, Brummeria, Pretoria, South Africa

**INTRODUCTION:** Previous work done by Jordaan *et al.*, 2008 [1] has developed a novel protein immobilization matrix, called dendrispheres. In this study, the dendrispheres are evaluated for their biocompatibility in *in-vitro* applications. Dendrispheres are an organic polymer based resin with an exceptionally high binding efficiency for proteins and have the potential for therapeutic applications. The use of any medical devices or protein delivering vehicles requires biocompatibility with body and body fluids [2] to prevent any injuries or damage by chronic inflammation or toxicity to the body or cells. This study therefore establishes a sterile manufacturing procedure of the dendrispheres to be endotoxin-free and determines the toxicity of the dendrisphere in an *in-vitro* cell culture system. Furthermore, the cellular immune response to the dendrispheres will be analyzed to obtain an indication of the dendrispheres biocompatibility in an *in-vitro* cell culture system.

**METHODS:** The manufacturing of dendrispheres has been outlined in the PCT application<sup>1</sup> outlining the polymerization of polyethyleneimine with the cross linking of glutaldehyde in an oil emulsion. An aseptic manufacturing method was established and the dendrisphere were gamma irradiated prior to their testing for endotoxins with the QCL-1000 Chromogenic LAL assay (Lonza). The biocompatibility of the dendrispheres will be established in three different cell culture systems: HeLa, HL60 and U937 cell lines. Cell cytotoxicity of the dendrispheres will be evaluated with the CytoTox-Glo Cytotoxicity Assay (Lonza). Furthermore, supernatant of the cell cultures will be analyzed for inflammation cytokines using CBA array (BD Bioscience) to determine whether the dendrispheres elicit an inflammation response.

**RESULTS & DISCUSSION:** We will present data indicating the biocompatibility of dendrispheres, including endotoxin, cell viability and cytokine data. The cytotoxicity assay measures the ratio of live/dead cells and thus can be used to evaluate the polymer's toxicity to cells *in-vitro*. Furthermore, the data presented will indicate

whether the dendrispheres elicit an immunogenic response and preventative measures taken to counteract these effects and ensure biocompatibility.

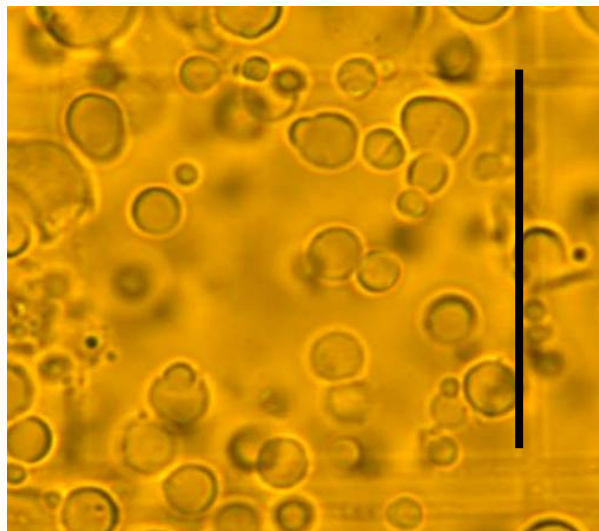


*Fig. 1: Protein immobilization matrix manufactured from polyethyleneimine in mineral oil emulsion polymerization. The measuring rod indicates 0.0625mm*

**REFERENCES:** <sup>1</sup>J. Jordaan, D. Brady, I. Gerber, and Gardiner, NS. 2008. PCT/IB2008/054458  
<sup>2</sup>Zeus® Biocompatibility of Plastics, ©2005 Zeus Industrial Products, Inc.

## Targeted Plasmid DNA Delivery by Galactosylated Alkyl-Oligoamine Derivatives of PEI

A. Dehshahri<sup>1,2</sup> R. K. Oskuee<sup>2,4</sup> W. T. Shier<sup>3</sup> & M. Ramezani<sup>4</sup>

<sup>1</sup> Department of Biotechnology, School of Pharmacy, Shiraz University of Medical Sciences, Shiraz, Iran. <sup>2</sup> Department of Modern Sciences and Technologies, School of Medicine, Mashhad University of Medical Sciences, Mashhad, Iran. <sup>3</sup> Department of Medicinal Chemistry, University of Minnesota-Twin Cities, Minneapolis, USA. <sup>4</sup> Department of Biotechnology, School of Pharmacy, Mashhad University of Medical Sciences, Mashhad, Iran

**INTRODUCTION:** DNA complexation into nanometric particles is a necessary prerequisite for efficient delivery of DNA into cells [1]. In the present study we have prepared a series of galactosylated alkyl-oligoamine derivatives of PEI and examined the effects on transfection efficiency and cytotoxicity. The approach used was to alkylate low-toxicity 10kDa branched PEI with a series of  $\omega$ -bromoalkylcarboxylates with different chain lengths, followed by forming amide linkages between the terminal carboxylate moieties and oligoamines such as spermine (SP), spermidine (SPD), ethylenediamine (EDA) and diethylenetriamine (DETA). Finally, lactose bearing galactose group was coupled to the modified PEI structures. These studies test the hypothesis that galactosylation of PEI in addition to hydrophobic modification of low toxicity PEI without reduction in primary amine content is an effective strategy for improving transfection efficiency of polycation-based non-viral vectors while maintaining low toxicity.

**METHODS:** First, PEI was reacted with a series of  $\omega$ -bromoalkylcarboxylic acids with different chain lengths. The primary amine groups which were lost when the PEI was carboxyalkylated were largely replaced by forming amide linkages between the carboxylic end groups of the grafted alkyl chains and a series of oligoamines. The reaction was allowed to proceed for 24 h at room temperature followed by dialysis against water to remove the unreacted materials. The binding strength of the modified PEIs to plasmid DNA and the size of the nanoparticles were measured with ethidium bromide (EtBr) exclusion assay and dynamic light scattering studies, respectively. Gene transfer ability and cytotoxicity of the modified PEI were evaluated using Neuro2A and HepG2 cells.

**RESULTS:** The results of EtBr exclusion analysis and dynamic light scattering studies indicated that all PEI derivatives were able to efficiently bind plasmid DNA and form nanoparticles in the range of 100 nm, respectively. The transfection efficiency of modified PEIs complexed with a luciferase reporter gene (pCMV-luc) in N2A murine neuroblastoma and HepG2 cells was increased to a level comparable to that of 25,000 Da PEI. The transfection data of galactosylated PEI indicates that this modifications enhanced the ability of 10 KDa branched PEI to transfer a reporter gene into the HepG2 cell line due to the abundance of the asialoglycoprotein receptor (ASGP-R) which is specific for hepatocytes [2]. The cell viability studies showed that all the modified polymers were non-toxic at the lowest polycation/plasmid ratios.

**DISCUSSION & CONCLUSIONS:** The most probable reasons for the improved transfection efficiency are a more favorable hydrophobic-hydrophilic balance and greater buffering capacity in the endosomal pH range due to the attached oligoamines, in addition to targeting through galactose. A hydrophobic environment may also contribute to endosomal release by making the endosomal membrane fragile as a result of acting as a sink for lipids spontaneously released from the endosomal membrane.

**REFERENCES:** <sup>1</sup> K. Sagara, S.W. Kim, (2002) *J Controll Rel* **79**: 271–281. <sup>2</sup> K. Kunath, A. von Harpe, D. Fischer, et al (2003) *J Controll Rel* **88**: 159–172.

**ACKNOWLEDGEMENTS:** The financial support provided by Mashhad University of Medical Sciences and Iranian Nanotechnology Initiative is greatly acknowledged.

## Peptide Modified Polyethylenimine as Vector for Gene Delivery

M Ramezani<sup>1</sup> H. Parhiz<sup>1</sup> & A. Hatefi<sup>2</sup>

<sup>1</sup> *Pharmaceutical and Biotechnology Research Institute and School of Pharmacy, Mashhad, Iran*

<sup>2</sup> *Department of Pharmaceutical Sciences, College of Pharmacy, Washington State University, Pullman, WA, USA*

**INTRODUCTION:** Polyethylenimine (PEI) is currently a popular synthetic polycation among non-viral gene delivery vectors. Vast majority of vectors based on PEI available today have other components like peptides to improve the transfection efficiency by overcoming major barriers in gene delivery pathway. In this study we have prepared two derivatives of Polyethylenimine by introduction of SV40 large T antigen and an SPKK-containing octapeptide repeat motif into PEI 10kDa.

**METHODS:** Branched PEI with molecular weight of 10 kDa was reacted with heterofunctional linker N-succinimidyl 3-(2-pyridyldithio) propionate (SPDP) to obtain dithiopyridine (DTP)-derivatized PEI (PEI-DTP). PEI-DTP then was mixed with SV40 large T antigen (with the sequence of CGGPKKKRKV) or SPKK-containing octapeptide repeat motif present in the c-terminus of histone H1 (with the sequence of CGGATPKKSTKKTTPKKAKK). The amount of released 2-thiopyridone (absorption wavelength = 343 nm) upon the SH-reaction was used for the direct quantification of the extent of -SH coupling. Polyplexes of pDNA and obtained polymers were characterized using Ethidium Bromide (EtBr) exclusion assay and dynamic light scattering studies. Transgene expression levels of DNA/modified PEI were measured by a luminometric assay using Neuro2A cell line. Cytotoxicity of DNA/modified PEI complex was evaluated by a MTT-based cytotoxicity assay.

**RESULTS:** The amount of peptide grafting were 8-10% of primary amines of PEI. The data of EtBr exclusion assay and dynamic light scattering studies showed that derivatives of PEI in this study efficiently condensed pDNA and the size of obtained nanoparticles were below 100 nm. *In vitro* transfection efficiency of DNA/modified PEI complex was increased significantly compared to transfection efficiency of DNA/unmodified PEI complex.

### DISCUSSION & CONCLUSIONS:

Modification of PEI with SV40 large T antigen and an SPKK-containing motif in this study resulted in vectors with higher transfection efficiency and optimal characteristics. These novel conjugates with high transfection efficiency, low toxicity and small size can be good candidates for further development for systemic gene delivery *in vivo*.

**ACKNOWLEDGEMENTS:** The financial support provided by Mashhad University of Medical Sciences and Iranian Nanotechnology Initiative is greatly acknowledged.

## Calcium phosphate mineralization in phosphatic brachiopods, and vertebrates

D.G.Reid<sup>1</sup> M.T.Neary<sup>1,2</sup> M.J.Mason<sup>2</sup> T. Frišćić<sup>1</sup> M.J.Duer<sup>1</sup> & M.Cusack<sup>3</sup>

<sup>1</sup>Depts. of Chemistry & <sup>2</sup>Physiol. Development & Neurosci., U. Cambridge, Cambridge UK.

<sup>3</sup>Dept. Geograph. Earth Sci., U. Glasgow, Glasgow UK.



**INTRODUCTION:** The brachiopods of the subphylum Linguliformae are unusual among invertebrates in using carbonate substituted fluoroapatite (francolite) instead of calcium carbonate to form their shells. As they on one hand and the vertebrates on the other almost certainly evolved the ability to use calcium phosphates as structural materials completely independently, new insights into the control of phosphatic biomineralization (templating molecules, crystallization propagation inhibitors) may emerge from a comparative study of the mechanisms of Lingulid and vertebrate biomineralization.

**METHODS:** *L. anatina* and *D. tenuis* shells, and francolite (museum no. GLAHM 111221), were powdered as is necessary for NMR and XRPD (Philips X'Pert Pro, Ni-filtered CuK<sub>α</sub> radiation); NMR methodology is described in Ref. 1.

**RESULTS:** Figure 1 compares <sup>13</sup>C spectra from the shells with that of chitin, a prominent

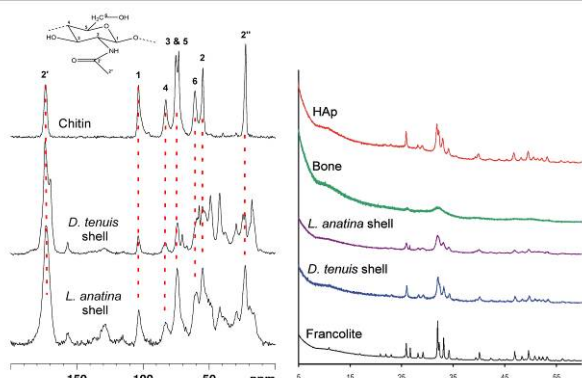


Fig. 1: Comparison of <sup>13</sup>C NMR spectra of brachiopod shell and chitin (left), and of XRP diffractograms of shell, bone, and macro-crystalline francolite and hydroxyapatite (right).

polysaccharide component of the organic matrix. XRPD shows that, in contrast to bone, Lingulid mineral is highly crystalline.

The <sup>13</sup>C{<sup>31</sup>P} REDOR NMR experiment probes the composition of the organic-mineral interface in phosphatic biominerals; it shows that this interface in vertebrate hard tissues [1,2] is comprised of glycosaminoglycans (GAGs). However our shell materials show no comparable organic-mineral atomic level association (Fig. 2).

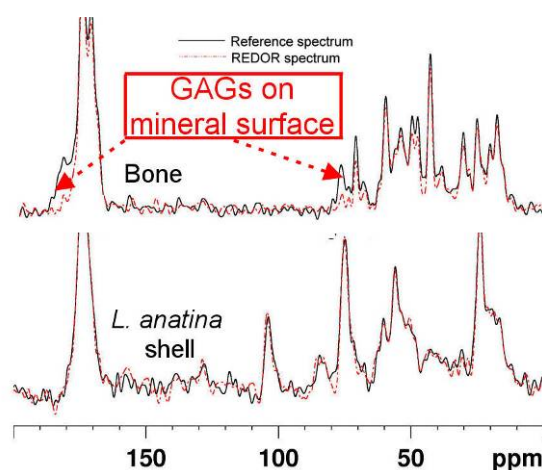


Fig. 2: Overlay of <sup>13</sup>C spectra without (black) and with (red) the mineral-organic phase magnetic interaction active. GAG signals disappear from the bone spectrum but there is no effect on spectra of either shell.

**DISCUSSION & CONCLUSIONS:** There are numerous significant differences between Lingulid and vertebrate biomineral. Lingulid fluoroapatite is more crystalline than vertebrate apatite, with no prominent organic-mineral atomic level interactions. The organic matrix composition does not appear highly conserved (cf. the spectra in Fig.1). Both organisms are adapted to highly specific habitats; their biomineralization strategies could not only help elucidate their evolutionary biology but also aid design of novel biomaterials

**REFERENCES:** <sup>1</sup>M.J.Duer et al. (2007) *Chem. Mater.* **19**:5055-7. <sup>2</sup>D.G.Reid et al. (2008) *Chem. Mater.* **20**:3549-50.

**ACKNOWLEDGEMENTS:** UK BBSRC; Dr. J.W.Faithfull, Hunterian Museum, U. Glasgow for francolite.

## A surfactant based approach to multi-functional, biocompatible polymer development

S. Govender<sup>1,2</sup> & P. Swart<sup>3</sup>

<sup>1</sup> *CSIR Built Environment, CSIR, Pretoria, South Africa.* <sup>2</sup> *Lehrstuhl für Technische Chemie II, Universität Duisburg-Essen, Germany.* <sup>3</sup> *Department of Biochemistry, University of Stellenbosch, South Africa*

**INTRODUCTION:** Biodegradable Pluronic® F108 and SDS are commercial EPA and FDA approved medical and food additives, capable of modifying polymer surfaces for both biospecific ligand binding and surface regeneration. Planar, piezoelectric poly (vinylidene fluoride) membranes were fabricated as solid adsorption matrices for non-covalent Pluronic surface modification and SDS regeneration [1]. Pluronic surfactants are PEO-PPO-PEO tri-block copolymers, which self-assemble onto hydrophobic surfaces via the hydrophobic PPO centre block, while the longer hydrophilic PEO chain forms a flexible tether that terminates in a functional hydroxyl moiety. In this work, the terminal hydroxyl group has also been covalently modified for ligand attachment and subsequent bio-specific protein binding from solution. The surface functionalised polymers described can also be re-used with an SDS based regeneration formulation.

**METHODS:** Hydrophobic PVDF membranes were fabricated using the phase inversion technique while the terminal hydroxyl groups of Pluronic were covalently modified to various ligands including a biotin derivative [2]. Ligand synthesis was confirmed with FT-IR and NMR analysis. Histidine pantothenate kinase (His<sub>6</sub>-PK) and avidin-HRP (Av-P) were immobilised on each affinity membrane respectively. This binding was also confirmed in mixed protein solutions and these bio-affinity membranes were regenerated and recoated to test both the durability of the affinity linker attachment mechanism and the efficacy of the regeneration solution [3].

**RESULTS:** The amphiphilic non-ionic surfactant Pluronic F108, was covalently derivatised to form novel ligands (halide and thiol derivatives for surface analysis), Pluronic-Biotin as a biochemical sensor and Pluronic-DMDDO for metal chelation. The multi-functional ligand coupling is illustrated in Fig.1. Micellar SDS formulations (34 mM) however, were much more effective in displacing adsorbed protein foulants (Av-P and lysozyme) and this was attributed to the conformational change in the protein structure after denaturation

by SDS micelles [2]. Additionally this SDS based regeneration system was shown to enable up to 4 cycles of repeated regeneration and re-use of Av-P immobilised PVDF~F108-biotin polymers.

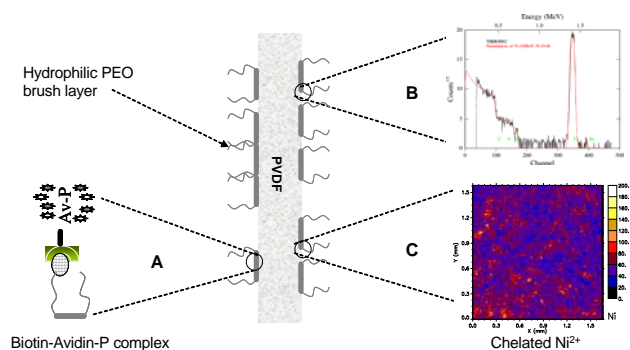


Fig. 1: Bio-functionalised PVDF polymers, inset A) the biotin-avidin-P complex formed on F108-biotin coated surfaces; inset B) RBS spectra of Br labelled Pluronic on PVDF and inset C) PIXE homogeneity map showing Ni<sup>2+</sup> distribution.

**DISCUSSION & CONCLUSIONS:** The synthesized derivatives exhibited typical Langmuir type adsorption on hydrophobic PVDF surfaces, and the saturation curves were similar to the unmodified parent compound. Furthermore F108 surfactants self-assembled onto hydrophobic polymers via the hydrophobic PPO centre block while the PEO chains formed a brush layer that hydrophilised the surface. Pluronic-biotin was able to bind specifically to avidin-peroxidase and the chelated Pluronic-DMDDO ligand can be used for affinity purification of histidine tagged proteins. A regeneration formulation based on anionic SDS detergent desorbed pluronic modified polymeric membranes and the possibility of re-usability increases the process lifetime of such biomaterials.

**REFERENCES:** <sup>1</sup> S.Govender and P.Swart (2008) *Colloids Surfaces A*, **331**: 97-102. <sup>2</sup> S.Govender, W.J. Przybylowicz, et al. (2006) *J. Membrane Science* **279**: 120-8. <sup>3</sup> S.Govender, E.P. Jacobs, M.W. Bredenkamp, et al. (2007) *J Chromat. B* **859**:1-8.

## Kidney stone composition by solid state NMR (SSNMR)

D.G.Reid<sup>1</sup> M.J.Duer<sup>1</sup> & G. Jackson<sup>2</sup>

<sup>1</sup>Dept. Chemistry, U. Cambridge, Cambridge UK. <sup>2</sup> Dept. Chemistry, U. Cape Town, Cape Town, South Africa.

**INTRODUCTION:** SSNMR is excellent for characterizing the composition of biomaterials; it can be quantitative and non-destructive and can often detect minor components which would be obscured to other techniques like XRPD and vibrational spectroscopy. Requisite SSNMR capabilities are increasingly common in academic and industrial laboratories.

**METHODS:** Human kidney stones were obtained from surgical procedures. Solid state NMR was conducted on a Bruker AVANCE-400 using standard methodology.

**RESULTS:** Figure 1 shows typical NMR spectra from kidney stone material. In terms of major features they are consistent with expectations

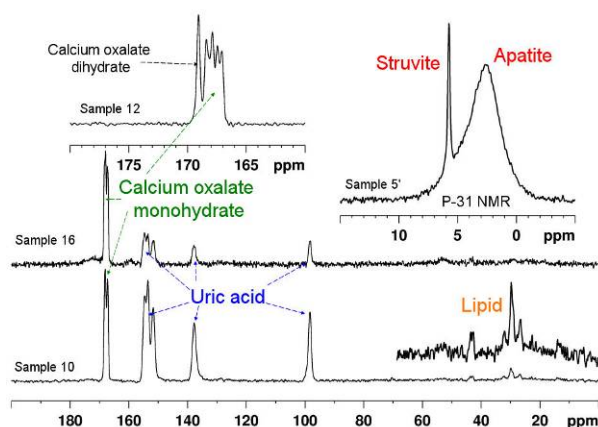


Fig. 1: Representative  $^{13}\text{C}$  and  $^{31}\text{P}$  NMR spectra of kidney stones. Note the presence of small amounts of lipid (Sample 10), uric acid (Sample 16) and struvite mineral (Sample 5).

based on XRPD. However the NMR reveals numerous minor features which would otherwise be unsuspected and go undetected.

Stones based on the calcium phosphate mineral apatite (similar to hydroxyapatitic material in healthy hard tissues like bone, and pathologically mineralized tissue like calcified atherosclerotic plaque) are particularly interesting. Unlike stones consisting primarily of organic salts or the ammonium magnesium phosphate mineral struvite, the apatitic stones entrain significant amounts of organic material. Also, a subpopulation of these macromolecules is involved in interactions at the atomic level with apatitic phosphate groups. This

is revealed by the double resonance NMR technique known as  $^{13}\text{C}\{^{31}\text{P}\}$  REDOR, in which  $^{13}\text{C}$  signals from functional groups less than 1 nm away from phosphorus atoms lose intensity. A typical result is shown in Fig. 2.

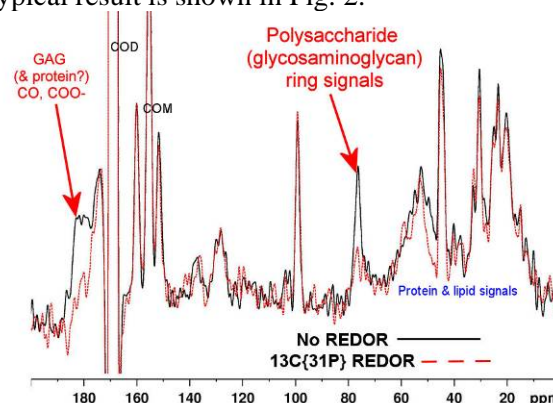


Fig. 2: Reference (black trace) and overlaid  $^{13}\text{C}\{^{31}\text{P}\}$  REDOR (red trace) spectra from an apatitic stone. Close atomic-range contacts between phosphate and organic groups cause the loss of signal intensity shown by the red trace.

**DISCUSSION & CONCLUSIONS:** We have previously used  $^{13}\text{C}\{^{31}\text{P}\}$  REDOR to show that the macromolecules lining the mineral-organic matrix interface in normally<sup>1</sup> and pathologically<sup>2</sup> mineralized tissue are polysaccharides, probably glycosaminoglycans (GAGs). This strongly implies a participatory rather than a bystander role for GAGs in calcium phosphate biomineralization, perhaps as templates or crystallization moderators. It is not clear whether, in pathological mineralization, GAGs are contributory to the pathological process, whether they are mobilized by the organism to inhibit undesirable mineral propagation, or whether their presence is merely coincidental. Kidney stones may provide a valuable new platform for studying fundamental mechanisms of biomineralization in disease, and its treatment.

**REFERENCES:** <sup>1</sup>M.J.Duer et al. (2007) *Chem. Mater.* **19**:5055-7. <sup>2</sup>M.J.Duer et al. (2008) *Arterioscl. Thromb. Vasc. Biol.* **28**: 2030-4.

**ACKNOWLEDGEMENTS:** UK BBSRC; Prof. Allen Rodgers and colleagues (U.C.T.) for stones.

## Synthesis of 1, 3- Propanediol From Sorghum

C M Obele<sup>1</sup> & O. Ogbobe<sup>2</sup>

<sup>1</sup>*Department Of Polymer And Textiles Engineering, Nnamdi Azikiwe University, Awka, Nigeria* <sup>2</sup> *Department Of Polymer And Textile Engineering, Federal University of Technology Owerri, Nigeria.*

**INTRODUCTION:** 1, 3- Propanediol (PDO) is the commonest diol used in Polyester Synthesis, Polyurethanes, Cyclic compound and as preservative for Cosmetic and Medical use.

**METHODS:** Dual enzyme technique was used to convert starch to sugar. Then glycerol was formed by fermentation of the sugar by yeast after 72 hours. Cultures of *Escherchia coli* and *klebsiella* specie were used to inoculate the glycerol obtained for final conversion to 1, 3- Propanediol. The mixture was left for 72 hours to ensure complete conversion. The reaction temperature for fermentation was 37<sup>0</sup>c. The expression of *Klebsiella* sp-diol dehydrates in *E-coli* catalyzed the conversion of glycerol to 1, 3- propanediol. The sample was then refiltered, distilled and condensed to obtain the pure, bio-PDO.

**RESULTS:** The bio-PDO synthesized was colourless and odourless. Specific gravity was 0.9992; purity was 99.92% by calculation. Table 1 shows the purity analysis by UV spectrophotometer. The boiling point was 121-123<sup>0</sup>c.

*Table 1. Purity Analysis using UV Spectrophotometer.*

Wavelengths (nm)	Expected Absorbance	Absorbance observed
220	< 0.200	- 0.291
250	< 0.075	- 0.294
275	< 0.075	- 0.298

**DISSCUSSION & CONCLUSION:** The PDO synthesized was found to be of comparable purity to chemically produced PDO.

**REFERENCES:** <sup>1</sup>J. Kurian, R. Muby & R. Miller (2005) Dupont Sorona Polymer <sup>2</sup> R.C Agu, M.U Okenchi, G. Aneke et al (1995). World journal of microbiology & Biotechnology II 591 – 592 <sup>3</sup> J.P. Dufour, Mellotte and S. Srebmik (1992). ASBC. J 50: 110-119.

## Determination of the Optical Properties of Rat Tissue

A Singh<sup>1</sup> A E Karsten<sup>1</sup> R M Smith<sup>2</sup> & G van Niekerk<sup>2</sup>

<sup>1</sup> Biophotonics Group, National Laser Centre, CSIR, P. O. Box 395, Pretoria, South Africa, 0001

<sup>2</sup> Dept Physiological Sciences, Stellenbosch University, Private bag X1, Matieland, 7602

**INTRODUCTION:** Many of the non-invasive methods for diagnostic and therapeutic modalities in biomedical applications are dependant on the interaction of light with tissue. Such interaction is influenced by the optical properties such as the absorption ( $\mu_a$ ) and reduced scattering ( $\mu_s'$ ) coefficients of the tissue. When consulting the literature however one finds there exists a huge discrepancy between measurements and an extensive database of optical properties is not available. Furthermore measurement of the *in vivo* tissue optical properties still poses some difficulty, however the Integrating Sphere (IS) system is one method which can be used to measure the optical properties of bulk tissue *in vitro*. This study thus involved investigating the optical properties of some tissue samples from rats.

**METHODS:** The setup currently has a 7.4 mW He-Ne laser ( $\lambda=632.8$  nm, JDS Uniphase laser) as the light source and is described in more detail in [1]. Tissue samples from Wistar rat (non-pigmented) were sandwiched between two microscope slides and held in place using parafilm and tape. Measurements of the total and diffuse transmission as well as the diffuse reflectance were taken in triplicates. Freshly excised, a day old, fridge and frozen samples were evaluated.

**RESULTS:** Figures 1 and 2 refer to the optical properties obtained from measurements on rat heart tissue samples using the experimental data and the multiple polynomial regression method [2]. The suffix 3 and 4 for both  $\mu_a$  and  $\mu_s'$  refer to the order of polynomial used in extracting the results, a and b refer to the different sides of the tissue.

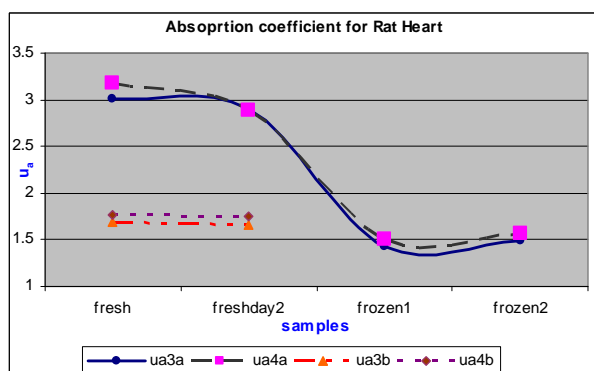


Fig. 1:  $\mu_a$  for different samples of rat heart

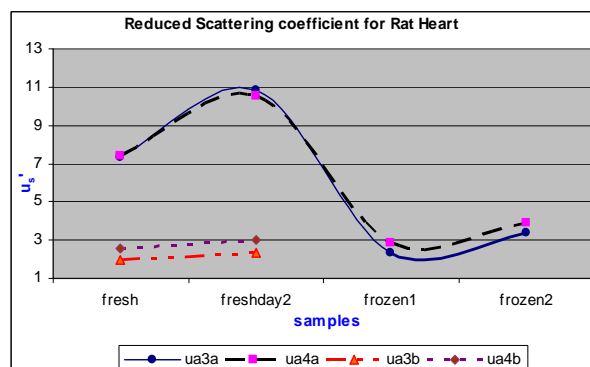


Fig. 2:  $\mu_s'$  for different samples of rat heart

In this particular instance there did appear to be a difference in the side of the tissue measured, which is consistent with the results obtained for the rat skin (to be published) but it is possible it may not always be true for all tissue types.  $\mu_a$  of the fresh sample and the same sample a day later shows a slight decrease. Furthermore the frozen samples show  $\mu_a$  to have decreased from 3 to 1.5  $\text{cm}^{-1}$ . There is a small increase in  $\mu_s'$  from 7 to 11  $\text{cm}^{-1}$  for the fresh sample after a day while  $\mu_s'$  for the frozen samples is 3  $\text{cm}^{-1}$ .

**DISCUSSION & CONCLUSIONS:** No literature values could be found against which to compare the extracted optical properties. However the change in  $\mu_a$  is expected due to the blood loss that occurs. The increase in  $\mu_s'$  could possibly be due to the disintegration occurring in the tissue that increases the scattering properties, while the low  $\mu_s'$  maybe a consequence of the freezing down process. These are preliminary results which will be investigated for a wider spectrum range. However it is evident that the state of a sample may influence the optical properties of some tissue.

**REFERENCES:** <sup>1</sup> A Singh, A E Karsten and J S Dam, (October 19-22 2008), *Proceedings of the International Conference of the World Association of Laser Therapy, Sun City, South Africa*, 165-169 ISBN 978-88-7587-471-1) <sup>2</sup> J. S. Dam, T Dalgaard, et al (2000) *Appl. Opt* **39** 1202-1209

**ACKNOWLEDGEMENTS:** The help of K Maduray in sample storage and retrieval is much appreciated as well as K Naidoo for critical review and the support of the NLC Biophotonics group.

## Improvement of cell-adhesion in the medical-surface boundary layer

Christiane Wetzel<sup>1</sup> N. Ozkucur<sup>2</sup> J. Schönfelder<sup>1</sup> T. K. Monsees<sup>2,3</sup> R.H.W. Funk<sup>2</sup>.

<sup>1</sup> *Fraunhofer Institute for Electron Beam and Plasma Technology (FEP), Dresden, Germany.*

<sup>2</sup> *Institute of Anatomy, University of Technology Dresden – Medical Faculty, Germany.*

<sup>3</sup> *Department of Medical Biosciences, University of the Western Cape, Bellville, RSA*

**INTRODUCTION:** Materials of medical products planned for applications in/on human bodies should be completely integrable in the proper milieu there. Especially polymers should perform optimized properties with regard to biocompatibility. For assessment of interactions in the medical surface boundary layer a thermodynamic well-founded **simulation model** has been developed. By use of it significant predictions are possible in prognosis and therefore efficient usage of technologies to improve surface properties.

**METHODS:** To confirm this simulation model polyurethane (PUR) was chosen as an example and the interactions with physiologic solutions of bovine serum, albumin and blood have been examined. For assessment of biocompatibility the parameters cell numbers, cell morphology, rate of apoptosis and cell proliferation did serve. By experiment mouse fibroblasts (L929) were incubated on modified PUR-samples. For improvement of surface properties, especially of surface energy and the polar portions, **non-thermal electron beam, plasma and ion-implantation technologies** have been applied.

**RESULTS:** By means of thermodynamic interpretation of adhesion work the wetting resp. adhesion could be predicted. Fig. 1 (at left) shows the iso-lines of adhesion work for untreated PUR and the bad wetting behaviour of blood. Surface modification by electron beam improved the results systematically, see Fig. 1 (at right). The values are in the optimum range.

**DISCUSSION & CONCLUSIONS:** Experimental studies, the thermodynamic interpretation by means of Free Standard Enthalpy  $\Delta_{\text{wet}}G^\circ$  of wetting as like as checks of biocompatibility and biofunctionality by in-vitro tests confirmed the results of simulation. Hereby a good conformity revealed between predictions based on the simulation and real cell behaviour. It is possible to aspire to

technical solutions for surface modification by using technologies mentioned above which enable an improved integration of synthetic polymers into the organism but also prevent degradation (biocorrosion) by humanbiological cell attacks. Resulting answers from simulation of cell adhesion create a spectra of multipurpose applications for prognoses in the medical-surface boundary layer.

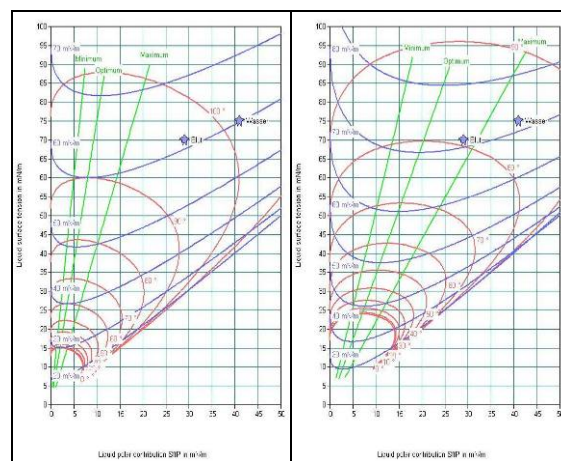


Fig. 1: Simulation model with iso-lines of adhesion work on untreated PUR (at left) and on electron beam treated PUR (at right).

**REFERENCES:** <sup>1</sup> C. Wetzel, F. Hollstein, R.H.W. Funk, N. Özkucur, T.K. Monsees, (2008) *Surf Coat Tech* **202**:5728-32.

<sup>2</sup> N. Özkucur, C. Wetzel, F. Hollstein et al. (2008) *J Biomed Mat Res A*, **89**(1):57-67.

**ACKNOWLEDGEMENTS:** This work was kindly supported in parts by a co-op project Grant No. 03 I 4040 A / InnoRegio BioMeT (Deutsche Forschungsgemeinschaft), by the BioMeT Sachsen Network and by the Board of FEP(Fraunhofer).

## Establishing A Platform For Spray Drying Inhalable vaccines In South Africa

[WA Germishuizen](#)<sup>1</sup> [L Venter](#)<sup>1</sup> [A Khosa](#)<sup>1</sup> [F Mudau](#)<sup>1</sup> [M Kabadi](#)<sup>2</sup> [A Schiermeier](#)<sup>2</sup> [DA Edwards](#)<sup>3</sup> & [PB Fourie](#)<sup>1</sup>

<sup>1</sup> [Medicine in Need South Africa \(Pty\) Ltd](#), Pretoria, South Africa. <sup>2</sup> [Medicine in Need Inc.](#), Cambridge, MA, USA. <sup>3</sup> [School of Engineering and Applied Sciences](#), Harvard University, Cambridge, MA, USA

**INTRODUCTION:** *Mycobacterium bovis* bacillus Calmette-Guérin (BCG) is the current vaccine for tuberculosis (TB). However, BCG as it is currently administered shows highly variable efficacy in protecting adults against TB. The natural route of infection of TB is via inhalation of bacilli-containing aerosols and it is postulated that immunization by the natural route of infection may lead to a greater immunity given the fact that the lungs are the primary target of infection. By eliciting both local and systemic immune responses, it is anticipated that an inhaled form of BCG will offer greater protection against pulmonary TB.

The Laboratory for Biomedical Aerosols at Harvard University, Cambridge, USA under the direction of Professor David Edwards has pioneered the application of spray drying to engineer drug formulations for pulmonary delivery [1-2]. With the appropriate choice of excipients and spray drying process parameters, large porous particles (LPPs) of drugs are produced with optimal physical properties for pulmonary delivery. The LPP technology has successfully been applied to anti-tuberculosis drugs, with inhaled capreomycin in early clinical development.

Current commercial BCG vaccine preparations are filled as bacterial suspensions in vials, dried through lyophilization and stabilized through refrigeration with a one year shelf life. However, freeze-dried BCG does not exhibit a particle form conducive for delivery via the aerosol route and must be injected. Thus, the LPP technology was applied to BCG as a means of effecting pulmonary delivery [3-4]. Spray drying studies at Harvard University have demonstrated that BCG could be spray dried into a viable aerosol with up to 1 year of stability under refrigerated conditions, and the potential for room temperature stability.

To support the further preclinical development of the BCG aerosol for application in the developing world, Medicine in Need established a state-of-the-art Biosafety level 3 spray drying facility with local expertise in South Africa, where the vaccine will be produced for an IND-enabling toxicology

study meeting OECD Good Laboratory Practice (GLP) requirements.

**METHODS:** Frozen BCG bulk is spray dried according to the methods developed at Harvard University [4] and the resulting dry powder is characterized in terms of viability and aerosol properties. Analytical methods include moisture content, geometric and aerodynamic particle sizing, and high performance liquid chromatography (HPLC) for determining chemical composition. The dried BCG aerosol is then aseptically filled into capsules using a semi-automatic filling device for delivery using a low-cost hand-held inhaler.

**DISCUSSION & CONCLUSIONS:** The spray drying technology was successfully transferred from Harvard University to the facility at the Medical Research Council (MRC) in Pretoria. Medicine in Need is developing local expertise and infrastructure to support further preclinical and clinical development of BCG for inhalation, and is currently investigating the application of the spray drying technology in formulating drugs and vaccines for pulmonary delivery in the treatments of TB, malaria and HIV.

**REFERENCES:** <sup>1</sup> D.A. Edwards, J. Hanes, G. Caponetti, et al (1997) *Science* **276**: 1868-71. <sup>2</sup> J. Fiegel, L. Garcia-Contreras, M. Thomas, et al (2008) *Pharm Res* **25**: 805-11. <sup>3</sup> Y.-L. Wong, S. Sampson, W.A. Germishuizen, et al (2007) *PNAS* **104**: 2591-95. <sup>4</sup> L. Garcia-Contreras, Y.-L. Wong, P. Muttill, et al (2008) *PNAS* **105**: 4656-60.

**ACKNOWLEDGEMENTS:** This work was supported by a Grand Challenges in Global Health grant for needle-free vaccine delivery from the Bill and Melinda Gates Foundation to Harvard University and Medicine in Need.

## Rapid Assessment Of Biomaterials: The HET-CAM Assay As Screening Tool For Biomedical Tissue Engineering

Claudia Eder<sup>1\*</sup>, Erwin Falkner<sup>2</sup>, Alexandra Slawik<sup>1</sup>, Michael Mickel<sup>1</sup>, Alexander Tuschel<sup>1</sup> & Michael Ogon<sup>1</sup>

<sup>1</sup>Orthopedic Hospital Vienna-Speising / Austria. <sup>2</sup>University of Vienna / Austria

**INTRODUCTION:** Prior to FDA approval of new biomaterials, careful biocompatibility assessment is required. Animal models are cost and time consuming, require a suitable facility, and trained animal caretakers and veterinarians. These premises make animal testing usually the last step in the research chain. The HET-CAM (Hen Egg Test – Chorionallantoic Membrane) test was originally validated for toxicity and irritation studies. The highly vascular nature of the chorionallantoic membrane (CAM) offers a complex testing environment for tissue reaction studies. Aim of the presented study was to test the suitability of the CAM for biocompatibility assessment of scaffold materials.

**METHODS:** 3 different scaffold materials (collagen sponge, collagen type I/III scaffold, collagen type II scaffold) and a  $\beta$ -Tricalciumphosphate bone graft substitute were applied onto the CAM. To evaluate the CAM model's potential to detect incompatible biomaterials, biocompatibility features were chemically altered using Ethidium Bromide. Evaluation was performed using a microscopic scoring system based on embryo viability, malformation, bleedings and vessel alteration. Histological and scanning electron microscopy analysis were applied.

**RESULTS:** Both collagen scaffolds showed excellent tissue integration. The scaffolds were soon infiltrated with blood vessels (Fig 1 a,c). The collagen sponge failed to integrate into the host tissue and demonstrated extremely rapid degradation at 37 °C, leading to a severe foreign body response (Fig 1 b,d). The highest neo-angiogenesis rate was achieved using the collagen type I/III scaffold, followed by the collagen sponge. The collagen type II membrane showed a vascularisation similar to untreated controls. Altering biocompatibility patterns led to a severe foreign body tissue response and could be clearly detected in histological analysis. The bone graft substitute showed a significant increase in angiogenesis, but demonstrated an alteration of the

surrounding connective tissue compatible with fibrous encapsulation.

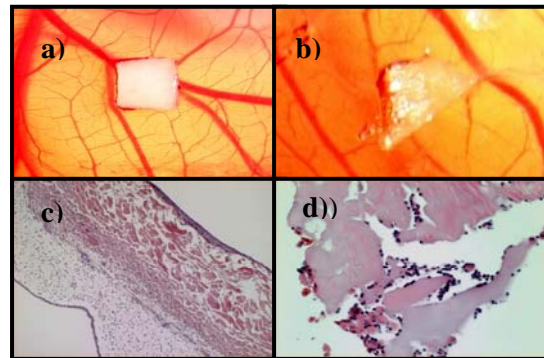


Fig 1.: a,c.: rapid tissue integration and neo-angiogenesis induced by a collagen type I/III scaffold. b,d.: Failed tissue integration, vessel bleeding and a foreign body reaction induced by extreme rapid degradation of the collagen sponge.

**DISCUSSION & CONCLUSIONS:** The study tested the potential of the HET-CAM test for biomaterial pre-evaluation prior to animal testing. The transplanted biomaterials showed rapid integration into the connective tissue of the CAM and gained connection to the embryonic blood stream – indicating that a simulation of transplant experiments, where a connection to the recipient's blood circulatory system is crucial for transplant survival – is actually possible. A 10 days old chicken embryo represents a partial immunodeficient model lacking a functional humoral immune response. However, a tissue reaction is possible allowing the distinction of biocompatible and incompatible materials. These results indicate that the HET-CAM test may serve as a rapid, cheap and simple model allowing a pre-assessment of biocompatibility patterns during the developmental process of scaffolds and biological implant materials for tissue engineering tasks.

## Optical Coherence Tomography as a Research Tool for Biomaterials

A E Karsten<sup>1</sup>, A Singh<sup>1</sup> and I Ndhundhuma<sup>1</sup>

<sup>1</sup>*Biophotonics Group, National Laser Centre, CSIR, P. O. Box 395, Pretoria, South Africa, 0001*

**INTRODUCTION:** Optical Coherence Tomography (OCT) is an imaging technique based on a Michelson's interferometer that allow penetration up to 3 mm in biological media. It fills the gap between confocal microscopy and ultrasound imaging. The applicability of Fourier-domain optical coherence tomography (FD-OCT) for probing of different biological materials to allow for real-time imaging is demonstrated. The advantages of 3-D imaging and non-destructive imaging are shown.

Optical coherence tomography (OCT) combines broad bandwidth near-infrared probe light and fiber-optic interferometry to probe optically opaque samples in reflection or backscattering mode and affords generating micron-scale resolution 2-D and 3-D spatial maps of various specimen microstructures without staining or chemical treatment<sup>1</sup>. In-situ non-destructive, non-invasive and non-contact probing is a major offering of OCT unlike routine optical methods often requiring extensive and costly sample preparation including mechanical sectioning. FD-OCT is the current generation of OCT instruments employing a high-speed wavelength-swept near-infrared laser probing light source, a spectrometer and Fourier transformation algorithms to generate depth-resolved 2-D images of the specimen under evaluation within a shorter period of time.

**METHODS:** In this study a commercial FD-OCT (Model OCM1300SS) by Thorlabs Inc., USA was used. This system has the following performance specifications: 1300nm centre operating wavelength, a 110nm 3dB spectral bandwidth, transverse spatial air resolution of 15- $\mu$ m, a depth spatial air resolution of <20  $\mu$ m, a probing depth of 3mm in air, >25mm working distance and acquisition time of 30 seconds for a sample volume measuring 512 pixels (L) by 512 pixels (W) and 512 pixels (D). Images of the samples were acquired as positive grayscale images. Strongly backscattering microstructures appear lighter (high signal intensity regions) while darker areas indicate weaker backscattering locations (low signal intensity regions). The imaging resolution of the system was verified with a USAF resolution target from Edmund Scientific, USA.

Abdominal skin samples of a euthanized, 32 days old Wistar rat were monitored over a 15 days. The samples were stored in a CO<sub>2</sub> incubator at 37°C in Eagle's minimal essential medium and just removed for imaging each day. The 3-D capability of the system is illustrated with an image of a moth and a PNIPAAm scaffold sample (experimental scaffold for growing cells).

**RESULTS:** Figure 1 shows the sectioning images through the rat skin (X-Z Plane). The degradation of the skin is clearly visible when the sample on day 4 is compared to that of day 15. A 3-D image of a moth is shown in Figure 2a and Figure 2b is the 3-D image of a PNIPAAm scaffold sample.

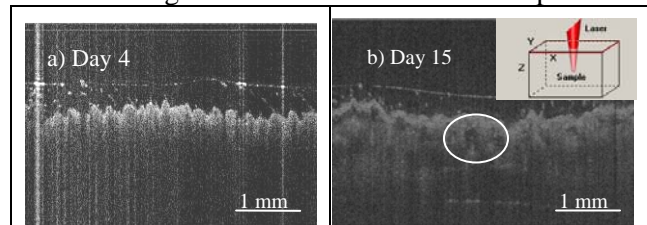


Fig. 1: OCT images of the degradation of rat skin over a 15 day period.

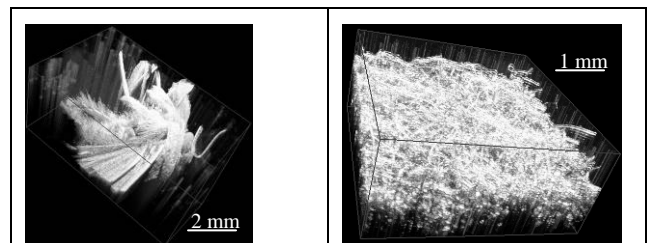


Fig. 2a: 3-D OCT image of a moth.

Fig. 2b: 3-D OCT image of PNIPAAm scaffold.

**DISCUSSION & CONCLUSIONS:** The results in Figures 1 and 2 show that it is possible to image sub-dermal changes in the structure of the skin samples as well as sub-surface structures. This imaging technique has proven to be a versatile non-invasive imaging tool for biological materials.

**REFERENCES:** <sup>1</sup>Mather ML (2007), Morgan SP, Crowe JA, *Regenerative Med.* **2**(2):145-160.

**ACKNOWLEDGEMENTS:** Thanks to the Dr D Goosen at Tshwane University of Technology (Labio) for the rat skin samples and A Chetty from MSM, CSIR for the PNIPAAm scaffold samples.

## Ca/Al Layered Double Hydroxides Hydrothermally Modified for Biomaterials Applications

[MS Azimi](#)<sup>1</sup> [ZT Birgani](#)<sup>1</sup> [A Darvish](#)<sup>1</sup> [SS Shafiei](#)<sup>1</sup> [MS Hashjin](#)<sup>1</sup>

<sup>1</sup>[Biomedical Engineering Department, Amirkabir University of Technology, Tehran, Iran](#)

**INTRODUCTION:** Layered Double Hydroxides (LDHs) are layered materials with a brucite-like structure in which some divalent cations are replaced by trivalent cations forming positively charged layers. Within these layers there are exchangeable anions along with water molecules.

Owing to the excellent properties including lamellar structure with nanosized interlayer space, positive charge; absorption, storing, carrying and release ability of anions; simple inexpensive synthesis and memory effect along with a good biocompatibility; these novel bioceramics have gained an extensive attention in biomedical applications such as drug and gene delivery systems.

In this paper the synthesis of Ca/Al LDHs along with hydrothermal post-synthesis modification and some of their characteristics that can affect their biological applications have been studied.

**METHODS:** Ca/Al LDH was prepared from calcium and aluminium nitrate salts with conventional coprecipitation method. Following one hour of hydrothermal treatment in 100° C, the powder was separated and dried by two different methods using an oven or a freeze dryer. Then X-ray Diffraction (XRD) analyses and Scanning Electron Microscopy (SEM) were exploited to characterize the powder.

**RESULTS:** As can be seen in the XRD patterns, (Fig. 1) Ca/Al LDH with high crystallinity is formed by coprecipitation method followed by a hydrothermal treatment and no undesirable impurity phases were detected.

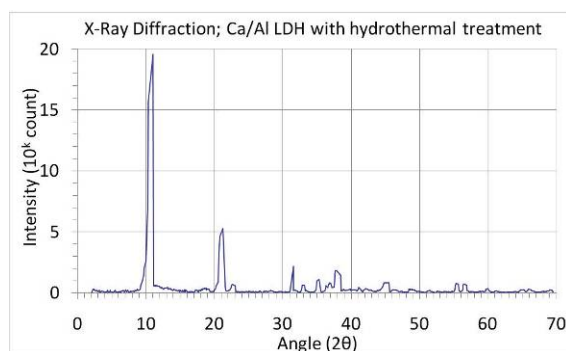


Fig. 1: XRD Pattern of the Ca/Al LDH formed (4h hydrothermal treated sample)

SEM images (Fig. 2) suggest that crystals with hexagonal morphologies and varied crystal sizes are formed.

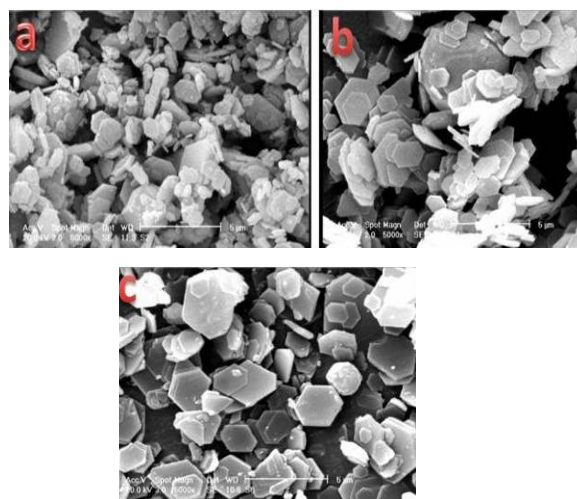


Fig. 2: SEM images of the Ca/Al LDHs hydrothermally treated for A) 4h b) 24h and c) 44h

**DISCUSSION & CONCLUSIONS:** Looking at the data obtained by XRD and SEM it is concluded that as the time of hydrothermal treatment increases, LDH crystals grow larger. The size distribution is significantly affected as well. The size distribution in samples, which were treated hydrothermally for longer periods of time stood within a narrower margin.

In conclusion, LDHs obtained via conventional coprecipitation method possess properties that can be further modified by hydrothermal treatment, particularly for specific biomaterials applications such as drug or gene delivery systems. However their interactions with cells and tissues and their other potential applications are yet to be investigated.

**REFERENCES:** <sup>1</sup> M.S. Azimi (2008) *Synthesis of anionic clays and their application as drug delivery systems*, Dissertation, Amirkabir University of Technology, Tehran, Iran. <sup>2</sup> J.H. Choy, et al(2007) *Appl. Clay Sci.* **36**: 122–132. <sup>3</sup> C.D. Hoyo(2007) *Appl. Clay Sci.* **36**:103–121.

## Application Of Low Level Laser On Skin Cell Lines

I M Ndhundhuma

CSIR, National Laser Centre, Biophotonics Group, P. O Box 395, Pretoria, South Africa, 0001

**INTRODUCTION:** Lasers have emerged as powerful tools for tissue engineering. To examine cellular growth, and cell to cell interactions, *in vitro* skin models have been developed combining two major cell types of skin, keratinocytes and fibroblasts. The main objective of the study is to construct 3D skin model for photodynamic therapy (PDT) investigation in skin cancers. Prior to using PDT on skin models, monolayer cultures are first used to investigate optimal dose of light and concentration of PDT drugs to be used for skin cells. In the current study, proliferation of cells (keratinocytes and melanoma), was evaluated for the possibilities of cancerous cells recovering after PDT treatment using low level laser light.

**METHODS:** Human skin keratinocytes (CRL2310) and melanoma (UACC62) cells were grown in their respective growth medium (Keratinocyte Basal Medium and RPMI medium) supplemented with growth factors (Whitehead Scientific). The cultures were incubated at 37°C with 5% CO<sub>2</sub> humidity. Cells were trypsinized using a 0.25% (w/v) trypsin-0.05% EDTA solution (Whitehead Scientific) and counted in a haemocytometer.

### Photosensitization of cells

Cells were seeded into 24 well tissue-culture plates at a density of  $3.0 \times 10^3$  cells/well (keratinocytes) and  $1.5 \times 10^3$  melanoma cells in 1 ml of KBM or RPMI medium, and allowed to attach for 48 hours before being washed twice with 2ml PBS, then photosensitized by the addition of serum-free medium without additives but only 10 µg/ml mixed-sulfonated zinc phthalocyanine (ZnPcSmix). Control wells contained medium without ZnPcSmix. Plates were incubated at 37°C in 5% CO<sub>2</sub> in the dark for 18 hours followed by irradiation with a diode laser with output power of 45 mW, with power density of 33 mW, at a wavelength of 672 nm for 30s. The diameter of the laser beam was 1.32 cm to give a laser dose of 1 J/cm<sup>2</sup>. Following irradiation, cells were cultured in their respective medium and returned to the incubator for further 72 hours. Cell morphology of treated and untreated cells were observed using an inverted microscope and digitally recorded.

### RESULTS:

Morphology of CRL2310 and UACC62 cells in culture was monitored under the inverted microscope at 32x magnification. The results indicated that addition of ZnPcSmix to normal human keratinocytes and cancerous melanoma cells exposed to 1 J/cm<sup>2</sup> diode laser, showed no proliferation of cells indicated by changes in cell morphology and detachment of cells from the surface of the flask, see Figure 1 (proliferation) and Figure 2 (no proliferation).

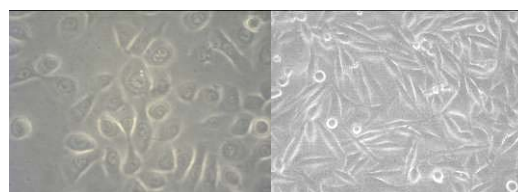


Fig. 1: Untreated keratinocytes (left) and melanoma cells (right).

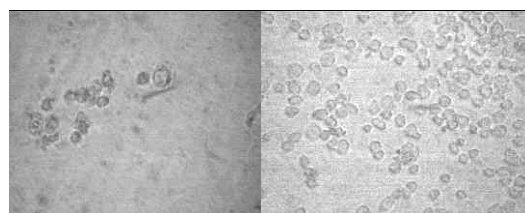


Fig. 2: Keratinocytes (left) and melanoma cells (right), 72hrs after PDT treatment

**DISCUSSION & CONCLUSIONS:** The results in Figure 2 (left) and (right) show that there is no proliferation of cells but cell death in PDT treated cells 72hrs post PDT treatment. Therefore low level laser can be a relevant medical device for treatment of skin diseases and tumors.

**REFERENCES:** <sup>1</sup>Fabris, C., Soncin, M., Miotto, G., Fantetti, L., Chiti, G., Dei, D., Roncucci, G. and Jori, G (2006) *Journal of Photochemistry and Photobiology Biology* **83**: 48–54. <sup>2</sup>Oleinick, N. L. and Evans H. H (1998) *Cellular Targets and Mechanisms Radiation Research* **150**(5): S146-S156.

**ACKNOWLEDGEMENTS:** This project was made possible by the CSIR, National Laser Centre; Prof. Heidi Abrahamse, Laser Research Group, University of Johannesburg; Ms N Kolesnikova, CSIR, Biosciences and Prof. Tebello Nyokong, Department of Chemistry, Rhodes University.

## Synthesis And Characterization Of Bisphosphonate Conjugated Carbon Nanomaterials As Potential Treatment Of Secondary Bone Cancer

N.L. Dlamini<sup>1</sup> X.Y Mbianda<sup>1</sup> Z. Szucs<sup>2</sup> & J.Zeervaart<sup>2</sup>

<sup>1</sup>Department of Chemical Technology, University of Johannesburg, Doornfontein Campus.

<sup>2</sup>Radiochemistry, The South African Nuclear Energy Corporation (NECSA), Pelindaba-District Brits

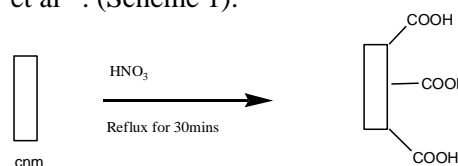
**INTRODUCTION:** Primary osteosarcoma (commonly referred too as bone cancer) accounts for 0.2% of all cancers with a mortality of 56%. Secondary bone metastasis is more prominent as 40-80% of breast and prostate cancer patients develop this painful situation. Forms of treatment include surgery, radiotherapy and chemotherapy. Chemotherapy is the most preferred form of treatment because the drug is distributed hence more effective in treating tumour lesions throughout the body. Numerous drugs are available but have a limited success due to poor target of the lesions ratios. Bisphosphonates (agent available for treatment) have a high selectivity for tumour bone lesions but are however, less potent if administered into the body system without the support of selective carrier system. This is due to the fact that bisphosphonates are metabolized by the hepatic system, then excreted before reaching the targeted tumor lesions. We wish to report here the synthesis of bisphosphonates conjugated double wall carbon nanotubes. We anticipate that the carbon material transport system will ensure that bisphosphonates reach their target sites as passive accumulation can be achieved through the enhanced permeability retention (EPR) effect where particles of a size less than 40 kDa cannot escape the normal vasculature but do so in tumour lesions where the blood vessels are ruptured. This reduces toxicity as less drug dosage will be administered into the body system.

**METHODS:** Our research can be divided into 4 sections: i) Synthesis of carbon nanomaterials (carbon nanotubes and spheres), ii) Oxidation of carbon nanomaterials iii) Phosphorylation of carbon nanomaterials iv) Characterization and testing of bisphosphonates conjugated carbon nanomaterial.

**RESULTS:** Carbon nanospheres and double wall carbon nanotubes have been successfully synthesized by pyrolysis of ethylene at 900°C and catalytic chemical vapour deposition ( $Mg_{0.9}Co_{0.1}O$  catalyst) respectively, as confirmed by

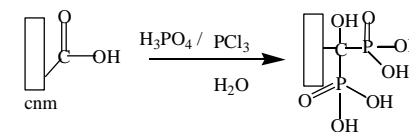
characterization techniques that include: Scanning electron microscope (SEM) and Transmission Electron Microscope (TEM).

Oxidation was carried out as described by R. Basca et al<sup>1</sup>. (Scheme 1).



Scheme 1: Oxidation of cnm

Oxidised carbon nanomaterials were phosphorylated through a literature modified method<sup>2</sup> as shown in scheme 2.



cnm = carbon nanomaterial

Scheme2: Phosphorylation of carbon nanomaterials

### DISCUSSION & CONCLUSIONS:

The functionalisation of CNTs were confirmed by EDX, IR, Raman and TGA analysis of the products obtained, for instance the presence in IR spectrum of peaks characteristic of P=O and P-O stretches at 1249 and 1049 $cm^{-1}$  respectively, was one proof that phosphoryl groups were successfully attached on the surface of the carbon nanomaterials.

**REFERENCES:** <sup>1</sup>R.R Basca, E Flahaut, C Laurent, et al (2003) New J Physics **5**:131.1131.9. <sup>2</sup>G.R Kieczkowski R.B Jobson, D.G Melillo, etal (1995) J Org Chem (1995)**60**:8310-8312.2.

**ACKNOWLEDGEMENTS:** Willie Augustyn (NECSA) and Mark Johnson (UJ) for their valuable advice, and UJ and NECSA for funding.

## Simple Drug Delivery System Based on PRP and PCL Nanofibres

R Jakubová<sup>1,2</sup>, A Míčková<sup>1,2</sup>, M Buzgo<sup>2</sup>, M Plencner<sup>1,2</sup>, E Prosecká<sup>1,2</sup>, E Filová<sup>1,2</sup>, & E Amler<sup>1,2</sup>

<sup>1</sup>*Department of Biophysics, 2nd Faculty of Medicine, Charles University in Prague, Prague, Czech Republic (CR).* <sup>2</sup>*Laboratory of Tissue Engineering, Institute of Experimental Medicine, Academy of Sciences of the Czech Republic, v.v.i., Prague, CR*

**INTRODUCTION:** Various nanofibre scaffolds such as PCL has become important devices in tissue engineering [1,2]. Commonly, nanofibres are implanted into the wound/defects seeded by cells only. Our aim was to prepare composite scaffold, where polycaprolactone (PCL) scaffold with adhered platelet rich plasma (PRP) was used as a cell support, to create a very simple drug delivery system. PRP was proved to enhance cell proliferation [3]. We studied the adhesion of PRP on PCL scaffolds by investigating of cell proliferation.

**METHODS:** PCL nanofibre scaffold was fabricated by electrospinning from chloroform/ethanol. PRP obtained from blood was purified and stored in liquid nitrogen before usage. PCL nanofibres was emerged into PRP solution for either 14 h (PCL14) or 2h (PCL2), respectively, to enable the adhesion, and seeded with  $20 \times 10^5$  chondrocytes. To compare, we investigated PCL without PRP (PCL) seeded with cells and PCL seeded with cells where PRP was added to the medium (PCLprp) (1:9) and cells seeded on tissue cell plastic (TCP) and TCP where PRP was added to the medium (1:9)(TCPprp). Cell proliferation was evaluated on the days 1, 7, 14, 21 by MTT assay. Quantitative data were presented as mean  $\pm$  SD (Standard Deviation). Results were evaluated statistically using One-Way Analysis of Variance (ANOVA), and the Student-Newman-Keuls Method. The level of significance was set at 0.05.

Cell viability was calculated as the percentage of live cells. Cells were incubated with 2',7'-bis(2-carboxyethyl)-5(6)-carboxyfluorescein acetoxymethylester (1 mM BCECF-acetoxymethyl ester, and, subsequently stained with propidium iodide. The scaffold was scanned using confocal microscope (BCECF- AM  $\lambda_{exc} = 488$  nm and  $\lambda_{em} = 505-535$  nm, Propidium iodide  $\lambda_{exc} = 543$  nm and  $\lambda_{em} = 630-700$  nm). Differentiation state of cells was determined by real time PCR for aggrecan and type II collagen genes.

**RESULTS:** The significant growth of cells was observed on day 7 and 14. Highest levels of absorbance were obtained on TCP on day 14.

On day 1 and 14, TCP showed significantly higher absorbance compared to other samples. Interestingly, the same absorbance value was observed on TCP and PCL2 on day 21, while other samples revealed significantly lower absorbance.

Cell viability according to LIVE/DEATH staining showed 90 % to 100 % viability of cells on all tested samples on day 1, 7, and 14. On day 21, cell viability decreased significantly in all types of scaffold except PCL2. Presence of type II collagen expression in chondrocytes was confirmed by real time PCR on day 1 and 14.

**DISCUSSION & CONCLUSIONS:** PRP on PCL2 scaffold effectively increased chondrocyte proliferation to the value of TCP on the day 21. On the other hand, PCL14 was not effective which was probably caused by lower enzyme activity due to the prolonged incubation. Interestingly, PRP on TCPprp inhibited cell proliferation compared to TCP.

The activity of PRP is influenced by the incubation time and the chemistry of the surface used. PRP is an effective tool for controlling cell proliferation and differentiation on PCL scaffold.

**REFERENCES:** <sup>1</sup>W.J. Li, K.G. Danielson, P.G. Alexander, R.S. Tuan, (2003) *J Biomed Mater Res A*. **67**(4):1105-14. <sup>2</sup>K.W. Ng, D.W. Huttmacher, J.T. Schantz, C.S. Ng, H.P. Too, T.C. Lim, T.T. Phan, S.H. Teoh, (2001) *Tissue Eng.* **7**(4):441-55. <sup>3</sup>E. Lucarelli, A. Beccheroni, D. Donati et al.(2003) *Biomaterials* **24**:3095-100

**ACKNOWLEDGEMENTS:** The study was supported by Grant Agency of the Czech Republic; grant numbers: 1ET400110403 and 304/05/0327, Ministry of Education, Youth and Sport of the Czech Republic; grant numbers: 1M0510 and NPV II 2B06130, research plan AV0Z50390512 and AV0Z50390703, Grant Agency of AS CR; grant number: IAA500390702 and Grant Agency of Charles University; grant numbers: 119009/2009, 122508/2008, 109708/2008 and 119209/2009.

## Contact Angle Studies on PDMS surfaces Fouled by Bovine Serum Albumin

*VT Windvoel<sup>1</sup> MB Mbanjwa<sup>1</sup> & K Land<sup>1</sup>*

*<sup>1</sup>Mechatronics & Micromanufacturing, CSIR Material Science & Manufacturing, PO Box 395 Pretoria, South Africa*

**INTRODUCTION:** Polydimethylsiloxane (PDMS) elastomer is growing to be a preferred material in microfluidics or life science applications[1]. This is due to its ease of fabrication, low cost, inertness, low toxicity and biocompatibility. Normally, PDMS has a hydrophobic surface, forming a contact angle of around 110° with deionised water. It is due to its hydrophobic nature that the elastomer is prone to bio-fouling, such as non-specific adsorption of biomaterials like proteins[2]. This is a limitation to microfluidic applications that require hydrophobic surfaces where proteins are involved. This study determines the change in wetting of PDMS after fouling by a protein, bovine serum albumin (BSA), by measuring contact angles.

**METHODS:** PDMS elastomer blocks were prepared by mixing a 10:1 ratio of Sylgard 184® silicone base and curing agent. The fluid mixture was cast into moulds, degassed for 30 minutes, and cured in an oven at 60°C for 2hours.

The contact angle studies were done on a surface under three conditions. The first condition PDMS was fouled with different BSA concentrations (50, 100 and 150 mg/ml) without pre-treatment. On the second condition the surface was precoated with mineral oil before fouling under the respective BSA concentrations. On the third condition, the surface was precoated with a solution of mineral oil with 50µl/ml an oil-soluble surfactant, Span 20®. Precoating was achieved by dipping the elastomer block in a petri dish containing the precoating fluid for 30 minutes.

The surfaces were then fouled by coating them with the different BSA solutions. The fouled PDMS surfaces were then dried in an oven at 60°C for an hour. A Skuor drop-shape analyzer was used to measure the contact angle of deionised water on the surfaces. The amount of BSA on each surface was qualitatively determined by looking at the surfaces under a light microscope.

### RESULTS:

*Table 1: Effects of coating & BSA Conc. on PDMS surfaces.*

Concentration	No coating	Oil	Oil + Span 20
50 mg/l	low	medium	high
100 mg/l	medium	high	Very high
150mg/ml	high	very high	Extremely high

*Table 2: Effects of PDMS coating on the contact angle.*

Concentration	Coating	Contact angle
clean	none	111.2°
50mg/ml	Oil	102.7°
50mg/ml	Oil-Span 20	100.6°
100mg/ml	Oil	98.5°
100mg/ml	Oil-Span 20	90.5°

**DISCUSSION & CONCLUSIONS:** An increase in BSA concentration resulted in a high amount of BSA accumulating on the PDMS surfaces. The other observation was that pre-coating the surface with oil and oil-Span 20 solutions also enhanced fouling. Contact angle measurements on fouled surface were difficult due to rough surface. The contact angle was not possible on the surface fouled with 150mg/ml BSA.

**REFERENCES:** <sup>1</sup> M.E Vlachpoulou, P.S Petrou, S.E Kakabakos, et al (2008) J Vacuum Sci & Tech. B **26**(6)  
<sup>2</sup> A.Mata, A.J Fleischman, S. Roy (2005) Biomed Microdevices **7**:281-293.

**ACKNOWLEDGEMENTS:** This work was funded by the Parliamentary Grant (PG) from CSIR Materials Science and Manufacturing. The authors would like to thank all the members of the NSIA MES Project and Mr. Itumelng Mputle for his assistance with contact angle measurements.

## Synthesis of Silicon Carbide Nanowires from a Hybrid of Amorphous Biopolymer and Sol-Gel Derived Silica

*AK Mishra<sup>1</sup> SB Mishra<sup>1</sup> BB Mamba<sup>1</sup> & RW Krause<sup>1</sup>*

<sup>1</sup>*Department of Chemical Technology, University of Johannesburg, Doornfontein, P.O. Box 17011, Johannesburg, Republic of South Africa*

**INTRODUCTION:** Silicon carbide (SiC) nanomaterials are widely investigated due to high strength, good creep, oxidation resistance at elevated temperature, chemical inertness, thermal stability and resistance to corrosion [1-3]. The size, shape and surface composition of these nanostructured materials are some of the few factors which contribute to these unique and fascinating properties [4-5]. These extraordinary properties allow silicon carbide to be a suitable ceramic for numerous applications such as semiconducting devices to be used at high temperature and high frequency, reinforcement in ceramic composites, metal matrix composites and catalytic support. Sol-gel process combined with the techniques such as polymer blending is used to fabricate the organic-inorganic hybrid materials for the production of composite nanomaterials such as SiC. In the sol-gel process and polymer blend technique, sol-gel derived silica was blended with coal tar pitch, polypropylene-polystyrene blend and polycarbonate to yield silicon carbide nanofibers.

**METHODS:** We report here the formation of silicon carbide (SiC) nanowires from inorganic-organic hybrid of sol-gel derived silica and the commercially available lignin which is naturally abundant amorphous biopolymer. Organic-inorganic hybrid material in the absence catalyst was carbothermally reduced for a period of 1 hr at 1400°C in inert atmosphere followed by oxidization.

**RESULTS AND DISCUSSION:** The crystallographic structure of the hybrid precursor & pyrolyzed-oxidised sample of lignin-MTEOS were analyzed by X-ray diffraction. The characteristic peaks of  $\beta$ -SiC appeared at  $2\theta = 35.5$  and  $60.2$  for the samples. The (111), (200), (220) and (311) diffraction peaks for  $\beta$ -SiC were also identified. A small shoulder indicating the stacking faults, commonly observed in SiC material confirms the crystalline nature of the pyrolyzed-oxidized sample.

The Raman spectrum for pyrolyzed-oxidised sample of lignin-MTEOS. The Raman shift due to SiC was not expected to be very sharp. The crystalline band appearing at  $983.1 \text{ cm}^{-1}$

corresponds to longitudinal optical peak and the band observed at  $795.6 \text{ cm}^{-1}$  indicate transverse optical peak. The broadening of the peak at  $795 \text{ cm}^{-1}$  could be results of the stacking faults of SiC.

The FTIR spectrum of the pyrolyzed-oxidised sample of SiC shows characteristic vibration of SiC at  $805 \text{ cm}^{-1}$ . The peaks appearing at  $475$  and  $100 \text{ cm}^{-1}$  are assigned to Si-O-Si and O-Si-O of unreacted silica as crystoballite.

Internal structures of SiC nanorods were obtained using transmission electron microscopy. HRTEM micrographs of the pyrolyzed and pyrolyzed-oxidised sample of SiC respectively. TEM micrograph of the pyrolyzed sample where SiC nanorods is in the native form. Upon calcinations at  $800^\circ\text{C}$  as shown in the amorphous carbon oxidises leaving behind the composite of SiC as core with an outer layer of silica coated along SiC nanorods. It has been reported that the formation of SiC itself acts as a diffusion barrier for carbon oxidation by hindering the oxygen penetration.

**CONCLUSIONS:** The current investigation has reported the growth of SiC nanorods, synthesized by the sol-gel process and polymer blend technique from the organic-inorganic hybrid of lignin and polysiloxane. The formation of  $\beta$ -SiC, grey-white product obtained, was confirmed by XRD and FTIR spectral analysis. The pyrolyzed sample was mixture of SiC nanorods, amorphous carbon and the unreacted silica. The average diameter of SiC nanorods were in the range of 50-200 nm with few micrometers long. The internal structure of the oxidised sample shows the deposition of silica layer along SiC nanorods at the outer surface.

**REFERENCES:** <sup>1</sup>R. Kamakaran, F. Lupo, N. Grobert, et al (2001) *Carbon* **42**: 1-4. <sup>2</sup>K. Okada, H. Kato, K. Nakajima (1994) *J Am Ceram Soc* **77**: 1691-1693. <sup>3</sup>X. Bao, M.R. Nangrejo, M.J. Edirisinghe (2000) *J Mater Sci* **35**: 4365-4372. <sup>4</sup>A. Thiaville, J. Miltat (1997) *Science* **284**: 1939-1940. <sup>5</sup>

**ACKNOWLEDGEMENTS:** Authors are grateful to the NRF and Mintek's / DST Nanotechnology Innovation Centre (NIC) and UJ.

## Phantom Skin Absorption Coefficients from Spectrophotometric and Integrating Sphere Methods: Preliminary Comparative Results

JE Smit<sup>1</sup> A Singh<sup>1</sup> ITshoke<sup>1</sup> AF Grobler<sup>2</sup> & RW Sparrow<sup>3</sup>

<sup>1</sup> *CSIR National Laser Centre, Pretoria, South Africa.* <sup>2</sup> *Unit for drug development and research, North-West University, Potchefstroom, South Africa.* <sup>3</sup> *CSIR Biosciences, Pretoria, South Africa*

**INTRODUCTION:** Minimalistic or non-invasive diagnosis and treatment of skin disorders requires accurate information regarding skin optical properties [1]. Spectrophotometric and Integrating Sphere (IS) methods are commonly used to extract information regarding absorption and scattering properties of samples, although in the field of skin optics the latter is used more widely [1,2]. The aim of this study is to extract and compare absorption coefficients of liquid skin phantoms with these two methods.

**METHODS:** Absorbance spectra of liquid phantom skin samples were measured with a UV-VIS spectrophotometer (Shimadzu UV-1650 PC) using standard 1 cm pathlength. The liquid phantoms consisted of green food dye (GFD) of specific absorption and added in varying concentrations to either 0.01% Intralipid (20%) or 0.1% Pheroid<sup>TM</sup> artificial vesicle aqueous stock solutions. Absorption coefficients ( $\mu_a(\lambda)$ ) were calculated from the Beer-Lambert law

$$\mu_a(\lambda) = A(\lambda) \ln(10)/L \quad [\text{cm}^{-1}] \quad (1)$$

where  $A(\lambda)$  is the wavelength dependent absorbance of the sample and  $L$  the pathlength (cm). Reflectance and transmission measurements were also taken for each sample using an 8 inch diameter Integrating Sphere (Labsphere) connected to a 7.4 mW He-Ne laser ( $\lambda=632.8$  nm) coupled into a multimode fibre (core diameter 62.5  $\mu\text{m}$ ). Sample holders with a diameter of 25 mm were connected onto the entrance and exit ports of the IS. The signal was used as input to the detector (Ocean Optics USB4000 spectrometer) using a fibre (600  $\mu\text{m}$  core diam, Ocean Optics). A calibration model with known  $\mu_a$  was created using Intralipid (20%) (scatter, non-absorbing) and black dye (absorber, non-scattering) solutions. The optical parameters were extracted from the calibration model using the Newton-Raphson method.

**RESULTS:** Absorbances measured with both methods displayed the Beer-Lambert law's linearity, although the IS method's absolute result values are about a factor 6 smaller (Fig. 1). Calculated  $\mu_a$  residual values of GFD in either

Intralipid (20%) or Pheroid<sup>TM</sup> suggested a difference in sensitivity between methods as the absorbance of the GFD was increased (Fig. 2).

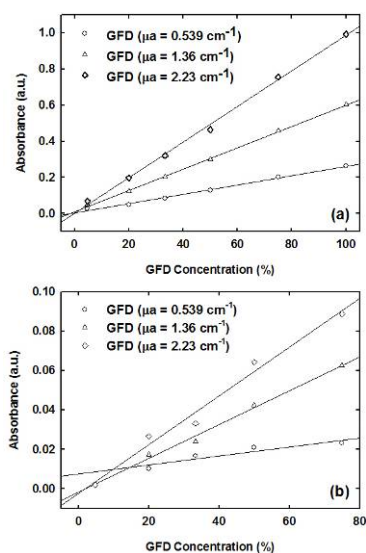


Fig. 1: Absorbance as a function of GFD concentration (in 0.1% Pheroid<sup>TM</sup> solution) for (a) spectrophotometric and (b) IS methods.

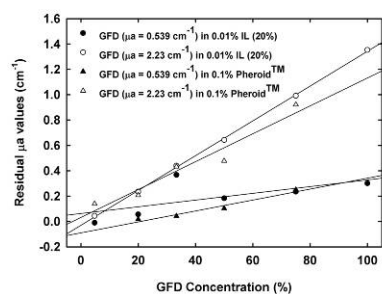


Fig. 2: Residual data between spectrophotometric and IS methods.

**DISCUSSION & CONCLUSIONS:** Preliminary results indicated similar trends with increased  $\mu_a$  values as GFD concentration and absorbance was increased. Differences in the methods' sensitivity may be due to shortcomings in the IS calibration model, or differences in measuring methodology with the two experimental set-ups.

**REFERENCES:** <sup>1</sup> B.J. Wilson, S.L. Jacques (1990) *IEEE J Quantum Electron* **33**:1471-77 <sup>2</sup> J.W. Pickering, S.A. Prahl, N. van Wieringen, et al (1993) *Appl Opt* **32**:399-410.

## Smart Biomimetic Matrices Induce Bone Formation without the Exogenous Applications of Soluble Osteogenic Molecular Signals

U Ripamonti<sup>1</sup> B van den Heever<sup>1</sup> LF Renton<sup>1</sup> PW Richter<sup>2</sup> & L Kotze<sup>2</sup>

<sup>1</sup>Bone Research Unit, Faculty of Health Sciences, MRC/University of the Witwatersrand, Johannesburg. <sup>2</sup>Materials Science and Manufacturing Technology, Council for Scientific and Industrial Research, Pretoria

**INTRODUCTION:** Regenerative medicine and tissue engineering of bone starts by erecting scaffolds of biomimetic biomaterial matrices that mimic the supra-molecular assembly of the extracellular matrix of bone. The molecular scaffolding lies at the hearth of all novel tissue engineering strategies. The insoluble signal, the carrier substratum which combined with the osteogenic proteins of the transforming growth factor- $\beta$  (TGF- $\beta$ ) superfamily, the bone morphogenetic/osteogenic proteins (BMPs/OPs) and uniquely in primates, the three mammalian TGF- $\beta$  isoforms, triggers the bone induction cascade.<sup>1</sup> The insoluble signal also provides an exciting and novel concept of tissue engineering, i.e. the development of biomimetic matrices that *per se* induce selected responses from invading mesenchymal stem cells. Can we design biomimetic matrices that *per se* can differentiate myoblastic endothelial stem cells into osteoblastic-like cells expressing selected mRNA species of the TGF- $\beta$  superfamily embedding the secreted osteogenic molecular signals into the biomimetic matrices?<sup>2</sup>

**METHODS:** Highly crystalline sintered hydroxyapatite (HA) and biphasic HA/ $\beta$ -tricalcium phosphate (HA/ $\beta$ -TCP) constructs were fabricated with a series of repetitive concavities assembled within the porous spaces of the macroporous samples. Solid discs of biphasic and/or highly crystalline HAs were also fabricated with a series of concavities on both planar surfaces and implanted in extraskeletal heterotopic *rectus abdominis* sites of adult non-human primate *Papio ursinus*. Macroporous constructs were also implanted in calvarial defects, 25 mm in diameter.

**RESULTS:** Morphological analyses of specimens implanted in the *rectus abdominis* muscle show vascular invasion and capillary sprouting with differentiation of mesenchymal stem cells in contact with the *smart* concavities. Bone differentiation by induction initiates by day 30 within the mesenchymal tissues that had invaded the concavities. Expression of mRNA species (Fig. 1A), i.e. OP-1, BMP-3, TGF- $\beta$ 1 and type IV collagen as evaluated by Northern blot analyses, is

followed by the embedding of the secreted gene products into the concavities of the biomimetic matrices (Fig. 1B) initiating in the induction of bone formation as a secondary response. Orthotopic specimens of HA/ $\beta$ -TCP showed substantial bone induction with dissolution/resorption of the implanted biomimetic matrices with complete regeneration (Fig. 1C).

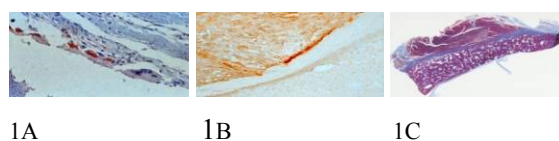


Fig. 1A: Localization of OP-1 in differentiating osteoblastic-like cells within a concavity of a biomimetic matrix; 1B: embedding of the secreted gene product into the biomimetic matrix; 1C: complete regeneration of bone across a 20/80 HA/ $\beta$ -TCP biomimetic matrix.

**DISCUSSION & CONCLUSIONS:** Our systematic studies in *Papio ursinus* have shown that the driving force of the intrinsic induction of bone formation by bioactive biomimetic matrices is the shape of the implanted scaffold; the language of shape is the language of geometry; the language of geometry is the language of a sequence of repetitive concavities that biomimetizes the remodelling cycle of the primate osteonic bone. The remodelling cycle entails a *resting* phase with quiescent resting cells over trabeculae of bone, *activation* phase, whereby osteoclastic cells are activated to resorb mineralized bone and the *formation* phase, whereby differentiating osteoblasts appear in the lacunae and pits cut by osteoclastogenesis inducing bone deposition within the concavities cut by osteoclastogenesis. The lacunae and concavities cut by osteoclastogenesis within the biomimetic matrices are the driving morphogenetic cues to induce bone formation in a *continuum* of sequential phases of resorption/dissolution and induction of bone formation.

**REFERENCES:** <sup>1</sup>Reddi AH (2000). *Tissue Eng* **6**: 351-9. <sup>2</sup>Ripamonti U (2004). *J Cell Mol Med* **8**: 169-80. <sup>3</sup>Ripamonti U *et al.* (2008). *J Cell Mol Med* **12**: 2609-21. <sup>4</sup>Ripamonti U (2009). *J Cell Mol Med* doi: 10.1111/j.1582.2008.00562.x

## Comparison of Osteoinduction in Biphasic Hydroxyapatite implanted in Two Different Animal Models

[LF Renton](#)<sup>1</sup> RB Parak<sup>1</sup> PW Richter<sup>2</sup> L Kotze<sup>2</sup> U Ripamonti<sup>1</sup>

<sup>1</sup> Bone Research Unit, Medical Research Council, University of the Witwatersrand, Johannesburg, South Africa.

<sup>2</sup> Materials Science and Manufacturing, Council for Scientific and Industrial Research, Pretoria, South Africa

**INTRODUCTION:** Tissue engineering requires three components: a soluble osteogenic molecular signal, a suitable insoluble substratum and responding host cells that are capable of differentiation into bone cells.<sup>1</sup> The morphogenesis of bone following intra and extraskelatal implantation of coral-derived porous hydroxyapatite was instrumental to the development of sintered highly crystalline hydroxyapatite/ $\beta$  tricalcium phosphate (HA/ $\beta$ -TCP) constructs capable of inducing bone formation *in vivo*. Studies have shown that the degradation or resorption of implanted HA/ $\beta$ -TCP ceramics by osteoclastogenesis is an important factor in osteogenesis and can be governed by adjusting the more soluble phase.<sup>2, 3</sup> Implantation of biphasic scaffolds in the non-human primate *Papio ursinus* yielded substantial bone formation by induction. Due to difficulties obtaining non-human primates as experimental animals it was decided to translate the research into more readily available animals such as Large White pigs (*Sus scrofa*).

**METHODS:** Hydroxyapatite and  $\beta$ -TCP powders were mixed in the ratio of 40/60 and 20/80 to form macroporous scaffolds for calvarial implants and monolithic discs for heterotopic muscle implantation. The discs were sintered, yielding a post-sinter phase content of 19/81 and 4/96 HA/ $\beta$ -TCP (wt %) respectively. Scaffolds were implanted in 4 adult baboons and 2 weaner Large White pigs. Both calvarial defects and muscle pouches in the *rectus abdominis* were used to ascertain the osteoinductivity of scaffolds. Histological and histomorphometric analysis was performed at 90 days (pigs and baboons) and 365 days (baboons) post implantation.

**RESULTS:** Baboon model: Morphological analysis of implants at both time periods revealed significant bone formation in and around implants at both bony and non-bony sites. At 1 year post-implantation, there was significant induction of

new bone with almost complete resorption/dissolution of the 4/96 calvarial specimens.

Large White pig model: Scaffolds of 4/96 HA/ $\beta$ -TCP were almost entirely resorbed in the calvarial defect sites. Only isolated islands of bone were seen, surrounded by fibrovascular tissue. Heterotopic implants showed limited bone formation by induction along two monolithic discs with the carved concavities.

**DISCUSSION & CONCLUSIONS:** Biphasic HA/ $\beta$ -TCP scaffolds performed favorably in the baboon model at 90 days, without the exogenous application of osteogenic proteins. Almost complete replacement by newly formed bone in the calvarial defect sites was seen. Conversely, the response in the Large White pig was not as expected within the same time frame, with rapid resorption of the scaffold and limited bone formation. The findings of this study highlight the potential pitfalls in translating the behavior of bioengineered scaffolds from one species to another, and that care must be taken when an animal model is selected for experimentation.

**REFERENCES:** <sup>1</sup>Reddi AH (2000). *Morphogenesis and tissue engineering of bone and cartilage: inductive signals, stem cells, and biomimetic biomaterials*. Tissue Eng **6**: 351-9  
<sup>2</sup>Daculsi G. (1998) *Biphasic calcium concept applied to artificial bone, implant coating and injectable bone substitute*. Biomaterials **19**:1473-8  
<sup>3</sup>Wenisch S, Stahl J-P, Horas U, Heiss C, Kilian O, Trinkaus K, Hild A, Schnettler R (2003). *In vivo mechanisms of hydroxyapatite ceramic degradation by osteoclasts: Fine structural microscopy*. J Biomed Mater Res. **67A**: 713-718

## Correlation of crosslink density with calcification of diamine-extended glutaraldehyde-fixed bioprosthetic heart-valve materials

Deon Bezuidenhout<sup>1</sup>, Anel Oosthuysen<sup>1</sup>, Paul Human<sup>1</sup>, Christoph Weissenstein<sup>2</sup> and Peter Zilla<sup>1</sup>  
<sup>1</sup>Cardiovascular Research Unit, University of Cape Town, South Africa. <sup>2</sup>Herzzentrum Osnabruck-Bad Rothenfelde, Schuechtermann-Schiller'sche Kliniken GmbH, Germany

**INTRODUCTION:** Despite much research into alternate chemistries<sup>1</sup>, glutaraldehyde (GA, at low concentrations) remains the reagent of choice for the commercial fixation of animal tissues used in bioprosthetic heart valves<sup>2</sup>. These tissues, however, remain susceptible to long-term failure due to calcific and inflammatory degeneration<sup>3</sup>. The current study investigates the effect of increased GA concentration and the extension of GA crosslinking with lysine, and correlates crosslink density with in vivo calcification of all three tissue types.

**METHODS:** Porcine aortic wall (PW), porcine aortic leaflet (PL) and bovine pericardial (BP) tissues were collected, dissected and rinsed immediately after slaughter. After initial fixation was performed in 0.2%; 1.0% and 3.0% GA in PBS for 48h, samples were placed into either (i) fresh solutions of corresponding GA concentrations for a further five days at 4 °C, or (ii) an L-Lysine solution (0.1M in PBS, pH 7.6, 37°C, 48h,) prior to continuation of the corresponding GA fixation. Samples were implanted into abdominal subcutaneous pouches in Long Evans rats (7 wk ± 1wk old) for 12 weeks, explanted, and evaluated for calcium content.

**RESULTS:** Lysine enhancement resulted in significant increases ( $p < 0.05$ ) in the DT of six out of the nine tissue/GA concentration combinations, and the RPD of 8 out of 9 treatments. Although an increase in GA concentration (without lysine) did not significantly increase the crosslink density, the RPD values for all tissues significantly improved when the GA concentration was increased in groups containing the lysine extension (PW:  $p < 0.0001$ ; PL:  $p = 0.0005$ ; BP:  $p = 0.0044$ ). The latter increase was much more marked for the PW (86%) than for the PL (13%) and BP (16%) when the GA concentration was increased from 0.2% to 3%.

When lysine was included in the crosslinking, the calcification of PW was significantly and dramatically decreased with increased GA concentration, while its effect on calcification of the other two tissue types was not significant. Incorporation of lysine resulted in significant (all  $p < 0.009$ ) decreases in calcification of all tissue types fixed at all the evaluated GA concentrations, with the exception of PW fixed at 1% GA. The largest effect of lysine enhancement was achieved when 0.2%

GA fixed pericardium was additionally treated with lysine: calcification decreased by more than 80 % from 183 to 34mg/g,  $p = 2 \times 10^{-6}$ ).

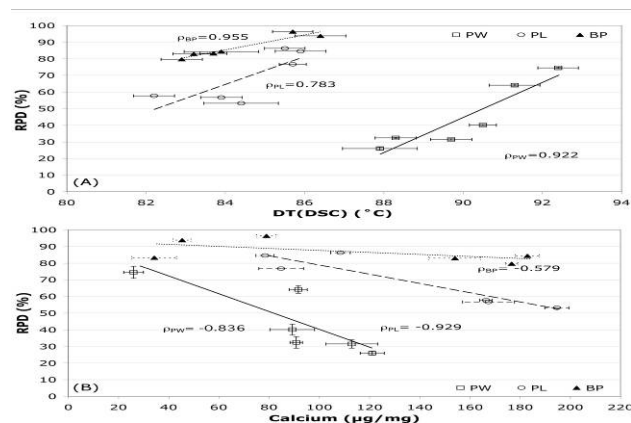


Fig. 1: Negative correlation of resistance to protease degradation (RPD) and calcification for the crosslinked tissues.

Strong inverse correlations were found between RPD and calcification for PW ( $r = -0.836$ ) and PL ( $r = -0.929$ ) tissues (both  $p < 0.05$ ), whereas the correlation for BP tissue was weaker ( $r = -0.579$ ; n.s)

### DISCUSSION & CONCLUSIONS:

It is thus concluded that the increase in crosslink density achieved by lysine incorporation, and by increased GA concentrations in the presence of lysine, results in significant and marked decreases in calcification of all three types of tissues commonly used in bioprosthetic heart valves.

**REFERENCES:** <sup>1</sup>Hendriks M, Everaerts F, Verhoeven M. (2001) *J Long Term Eff Med Implants*. **11**(3-4):163-183. <sup>2</sup>Jayakrishnan A, Jameela SR. (1996) *Biomaterials*. **17**(5):471-484. <sup>3</sup>Zilla P, Human P, Bezuidenhout D. (2004) *Biotechnol Appl Biochem*. **39**(I-II).

**ACKNOWLEDGEMENTS:** This work was supported by collaborative funding from Medtronic Inc., and by a grant from the Technology and Human Resources for Industry Program (THRIP) TP2004101400025, National Research Foundation, South Africa.

## Photochemically crosslinked proteins as new medical materials

CM Elvin<sup>1</sup>, AG Brownlee<sup>1</sup>, SJ Danon<sup>2</sup>, GA Edwards<sup>3</sup>, NE Liyou<sup>1</sup>, JAM Ramshaw<sup>4</sup>, L Sando<sup>1</sup>, T Vuocolo<sup>1</sup> and JA Werkmeister<sup>4</sup>

<sup>1</sup> CSIRO Livestock Industries, Queensland Bioscience Precinct, St Lucia 4072, Australia. <sup>2</sup> CSIRO Molecular and Health Technologies, North Ryde 2113, Australia. <sup>3</sup> University of Melbourne, Faculty of Veterinary Science, Veterinary Clinic and Hospital, Werribee 3030, Australia. <sup>4</sup> CSIRO Molecular and Health Technologies, Clayton South 3169, Australia

**INTRODUCTION:** We have previously reported the generation of a highly elastic, crosslinked protein biomaterial via a rapid photochemical process using visible light illumination that leads to the formation of intermolecular dityrosine crosslinks<sup>1</sup>. We expected that other tyrosine-rich proteins may also be susceptible to this crosslinking method. Here we show that native fibrinogen<sup>2</sup> or gelatin can also be photo-crosslinked and provide novel protein-based biomaterials. These photo-crosslinked proteins form tissue sealant bonds at least 5-fold stronger than commercial fibrin glue and can produce maximum bond strength within 20 seconds. These materials can also be used as scaffolds for growth and/or delivery of cells.

**METHODS:** Fibrinogen was from Sigma or prepared from bovine plasma. Gelatin was either bovine type B, or porcine type A (Sigma) and were used as 10-15% solutions in PBS. Ruthenium trisbipyridyl chloride [Ru<sup>II</sup>(bpy)<sub>3</sub>]<sup>2+</sup>Cl<sub>2</sub> and sodium persulphate (SPS) were from Sigma. Photo-crosslinking of fibrinogen or gelatin was carried out with 1mM [Ru<sup>II</sup>(bpy)<sub>3</sub>]<sup>2+</sup>Cl<sub>2</sub> and 10mM SPS by illumination for 20 sec with a 300W xenon lamp. Adhesive strength was assessed using an Instron 5544 using a bovine amnion membrane model. *In vitro* studies on various formulations included chondrocytes, fibroblasts or myoblasts. Porous scaffolds were formed by either chemical or enzymatic foaming. *In vivo* studies using rat and porcine surgical models were carried out according to CSIRO/University Animal Ethics procedures.

**RESULTS:** Both proteins are effectively and rapidly crosslinked by this photo-crosslinking process. Using this photo-crosslinking procedure, proteins can be molded, cast or extruded into various shapes including sheets, tubes, rings, spheres, rods and fibres. Also, when gelatin, which is a convenient and cheap protein substrate, is used as an adhesive the bonding was found to have a high intrinsic strength (~ 100kPa), good adhesion strength (~ 100kPa) and high strain to break (>500%) (Fig. 1). *In vitro* studies showed

that components of the photochemical crosslinking reaction are both non-toxic to cells. Initial wound repair studies demonstrate effective wound healing in a number of *in vivo* studies, including dermal repair, vascular and thoracic arterial haemostat sealant, dural repair and lung sealant.

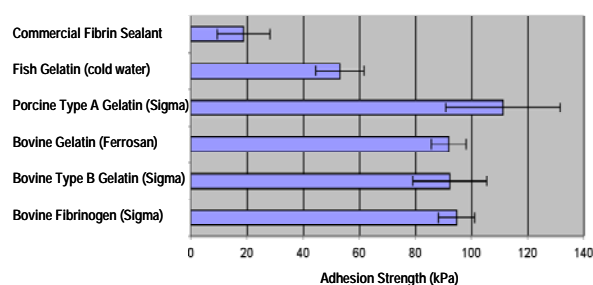


Fig. 1: Comparison of adhesion strengths of various photo crosslinked formulations compared to fibrin adhesive.

This photo-crosslinking method has also been used to generate scaffolds for cell growth. The process allowed scaffolds to be made in the presence of cells and growth factors in various shapes and forms. Various cells have demonstrated the efficacy of this process and the suitability to regeneration of selected tissues.

**DISCUSSION:** This study has described an easy method to effect rapid covalent crosslinking of fibrinogen or gelatin. The mechanical and biological properties of the material make it an excellent candidate for use in many medical applications where an elastic, rapidly-curing, biodegradable, high strength tissue bond is required.

**REFERENCES:** <sup>1</sup> C.M. Elvin *et al.* *Nature* (2005); **437**: 999-1002. <sup>2</sup> C.M. Elvin *et al.* *Biomaterials* (2009); **30**: 2059-2065.

## Determining the applicability of the SphereZymes® Immobilised Protease for the biocatalysis of Protein

LG Molawa<sup>1</sup>, D Brady<sup>1</sup>, J Jordaan<sup>1,2</sup>

<sup>1</sup>CSIR Biosciences, Enzyme Technologies, Private Bag X2, Modderfontein, 1645,

<sup>2</sup>CSIR Biosciences, Molecular Biomaterials, Synthetic Biology ERA, PO Box 395, Pretoria, 0001

**INTRODUCTION:** The Spherezymes Technology involves emulsification of enzyme solution (hydrophilic phase) in a hydrophobic phase (oil). This technology offer several advantages over other immobilisation technologies. For instance elicits size control by controlling the surface area to volume ratio and partial purification of the enzyme is required<sup>1</sup>. However, one of the primary drawbacks is its lack of applicability to enzymes catalysing bulky substrates.

**PARTIAL PROTEIN PURIFICATION:** Alcalase was partially purified through dialysis and cation exchange (CM Sepharose). The fractions with the highest alkaline protease activity as well as protein content were used for Spherezymes manufacture.

**SPHEREZYMES MANUFACTURE:** A 200 µl protein solution (100 mg/l) was reacted with a 50 µl active site protectant (2.5 % casein in ddH<sub>2</sub>O) for 5 min. Thereafter various cross-linking reagents (fig. 1) were added to the protein mix and immediately the resulting solution was emulsified in the oil phase. The oil phase comprised chilled 5 ml mineral oil and 50 µl nonoxynol. The Spherezymes were recovered through centrifugation and subsequently washed with 50 mM Tris buffer pH 8.

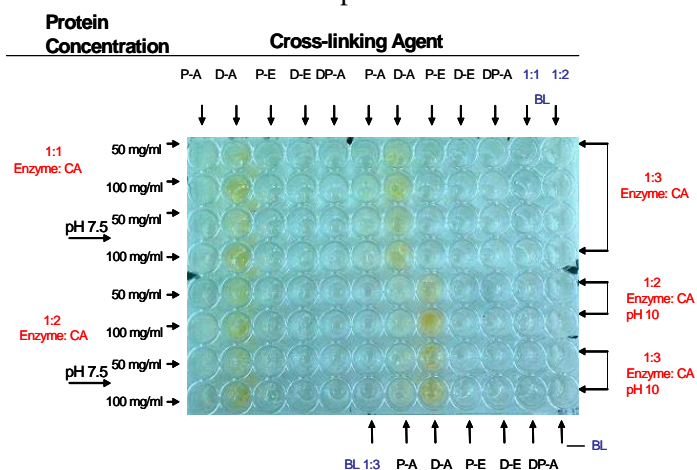


Figure 1. The effect of long spacer arm cross-linkers against bovine serum albumin. Dextran Aldehyde (D-A) showed cross-linking as seen by solidification and colour formation.

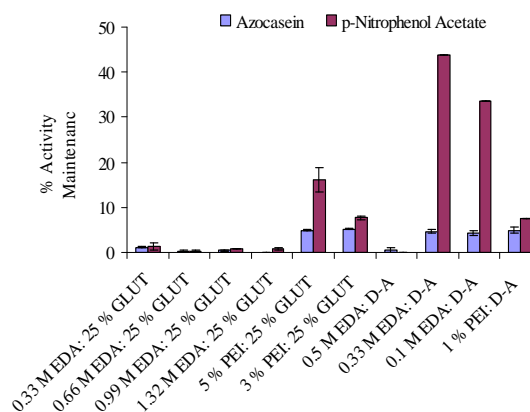


Figure 2. % activity maintenances of spherezymes with longer protein cross-linking agents. EDA- Ethylenediimine, GLUT- Glutaraldehyde, PEI- Polyethyleneimine, D-A- Poly-dextran aldehyde.

**DISCUSSION AND CONCLUSION:** The introduction of a longer spacer arm cross-linkers increased the activity maintenance toward both substrates. PEI is a poly-cation, being more nucleophilic at alkaline pH and theoretically more aldehydes from glutaraldehyde were available for enzyme coupling. Optimisation of inter cross-linking with dextran aldehyde and PEG aldehyde still need to be considered in order to increase the activity maintenance toward bulky substrates. These polymers were also reported to have positive effect toward activity and stability of other immobilised enzymes<sup>2</sup>.

**REFERENCES:** <sup>1</sup>Brady, D., Jordaan, J., Simpson, C., Chetty, A., Arumugam, C. and Moolman, F.S., 2008. *BMC Biotechnology*, **8**:8.

<sup>2</sup> Betancor, L., López-Gallego, F., Hidalgo, A., Alonso-Morales, N., Fuentes, M., Fernández-Lafuente, R. and Guisán, J.M., 2004. *J Biotech*, **110**(2): 201-207.

**ACKNOWLEDGEMENTS:** ZA Biotech for funding of research. Dr. J. Rashamuse and Mr. D. Visser.

## Scaled Manufacture of Self-immobilised *Pseudomonas fluorescens* Lipase Using the SphereZymes™ Technology

K. Mathiba<sup>1</sup>, B. Petja<sup>1</sup>, C. Simpson<sup>1</sup>, J. Jordaan<sup>2</sup>, & D. Brady<sup>1</sup>

<sup>1</sup>CSIR Biosciences, Private Bag X2, Modderfontein 1645, South Africa, <sup>2</sup>CSIR Synthetic Biology ERA, P.O. Box 395, Pretoria 0001, South Africa.

**INTRODUCTION:** SphereZymes™ technology employs support-free enzyme immobilisation which is achieved using an emulsification process. Through the addition of protein cross-linking to a water-in-oil emulsion of an aqueous enzyme solution, this technology allows for the formation of permanent spherical catalytic macro-particles (SphereZymes™)<sup>1</sup>. The technique is comparatively inexpensive and can provide stable and structured biological catalysts. This research outlines manufacturing of gram quantities of *Pseudomonas fluorescens* lipase SphereZymes™.

**METHODS:** *Pseudomonas fluorescens* lipase (Amano AK SD Conc.) was partially purified by precipitating with 60 %m/v PEG 6000, ultrafiltration with deionised water and lyophilising. SphereZymes™ were manufactured using the standard method<sup>2</sup> with the constituents as outlined in Table 1.

Table 1. Constituents for *Pseudomonas fluorescens* lipase SphereZyme™ formation and volumetric concentrations

Emulsion Constituent	% v/v
Mineral oil	93.98
Surfactant (NP4)	0.94
Protein: Enzyme (100 mg.ml <sup>-1</sup> ); Bovine Serum Albumin (10 mg.ml <sup>-1</sup> )	3.76
Enzyme active site protectant (Menthol)	0.94
Protein Crosslinker (Glutaraldehyde:Ethylenediamine at 1:1 ratio)	0.38

After centrifugation to break the emulsion and washing, lyophilisation of the particles was performed using a Genesis series freeze drier (Virtis). Samples were aliquoted into 5 ml volumes in vials with freeze drying seals and lyophilised over 3 days.

**RESULTS:** Partial purification of *P. fluorescens* lipase (50 grams) resulted in a mass recovery of ~ 44% and 2.53 -fold purification and a mass recovery of ~ 67% purification on *p*-nitrophenolbutyrate (PNPB). The activity recovery at

each purification step is shown in Figure 1. The lipase activity retained across purification for tributyrin was calculated to be ~72% (as compared to the starting concentration) achieving a 3.14 fold purification equating to 9.66 U. mg<sup>-1</sup>.

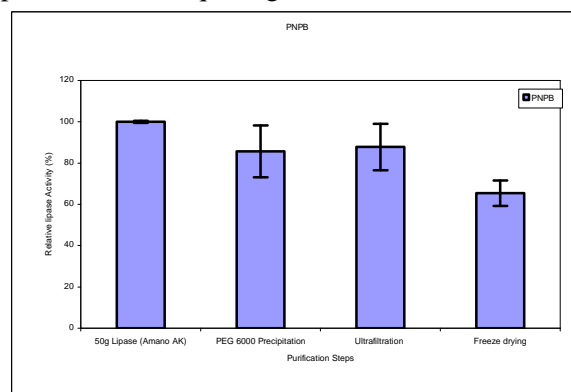


Fig. 1: Partial purification of lipase (based on cleavage of PNPB).

**DISCUSSION & CONCLUSIONS:** The manufacture of *Pseudomonas fluorescens* lipase SphereZymes™ was successful. Lipase SphereZymes™ were reproducibly produced with only ±7% variation at bench scale (3 x 1 litre batches). Dried (~ 2.14 g) particles with a total activity of ~4000 U. mg<sup>-1</sup> lipase (tributyrin) were recovered. Based on the small molecule assay (PNPB), approximately 24% of the activity of the partially purified enzyme was retained in the freeze-dried immobilized enzyme product.

**REFERENCES:** <sup>1</sup> F.S. Moolman, D. Brady, A.S. Sewlall, H. Rolfes and J. Jordaan (2005). *Stabilization of Enzymes*. WO2005080561  
<sup>2</sup> D. Brady, J. Jordaan, C. Simpson, C. Arumugam, A. Chetty and S. Moolman., (2008). *BMC Biotechnology* 8: 8.

**ACKNOWLEDGEMENTS:** We would like to thank ZA Biotech and Biopad for financial support.

## Thrombogenicity of Ti(N,C,O) diffusive coating layers developed on Titanium alloy as the blood contact surface.

M Gonsior<sup>1</sup> T Borowski<sup>2</sup> E Czarnowska<sup>3</sup> M Sanak<sup>4</sup> R Kustosz<sup>1</sup> M Ossowski<sup>2</sup> T Wierzchon<sup>2</sup>

<sup>1</sup>Foun. for Cardiac Surgery Development, Zabrze; <sup>2</sup>Technical University Warsaw, Warsaw; <sup>3</sup>Children Health Hospital, Warsaw; <sup>4</sup>Collegium Medicum Jagiellonia University, Krakow; Poland

**INTRODUCTION:** The original extracorporeal pulsatile heart support device, called POLVAD, has been developed in Poland. It was used in over 200 patients with the longest duration exceeding 6 months.

The innovative tilting disc valve for this device is developing. The valve consists of original valve ring, free of pivot element crossing the blood stream. The ring is made of Titanium alloy with surface modified by different surface treatment to obtain the lowest thrombogenicity.

**METHODS:** The three diffusive layers were tested as the blood contact surfaces: TiN+Ti<sub>2</sub>N+αTiN, TiO+Ti<sub>2</sub>N+αTiN, and Ti(OCN)+Ti<sub>2</sub>N+αTi(N).

The layer were produced under glow discharge conditions on titanium alloys samples of 14 mm diameter and 3 mm thick. The 3 μm coating layer exhibited a nanocrystalline structure and uniform low roughness.

The surface layers thrombogenicity after plasma and gas sterilization was examined in static and dynamic condition. In the static flow condition test, coated disc surface was exposure for 2 and 12 hours to reach platelet plasma. In dynamic share stress test, the surface of disc was exposure to 130 μl of whole blood rotating with the speed of 720 rpm within 300 seconds. The number of Platelets, Platelets Aggregates, Small and Big Platelets Aggregates, and Platelet Activation Level were examined utilizing Flow Cytometry, Fluorescent Microscopy, and Scanning Electron Microscopy.

**RESULTS:** Figures bellow show: the clinical POLVAD device and developing new valve.



Fig. 1: The POLVAD device (left) and valve (right).

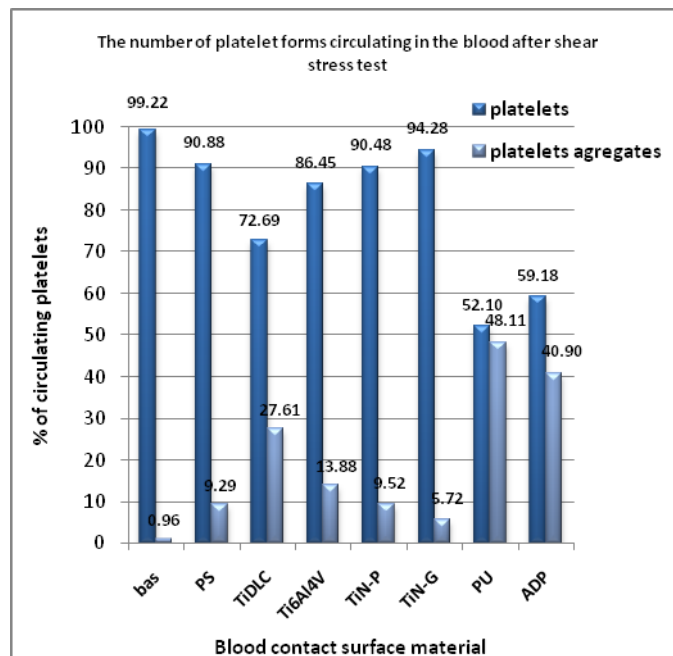


Fig.2: Relative platelets aggregation in blood exposed to shear stress. Bas – blood not exposed to shear stress, PS-polystyrene; TiN-P – Titanium Nitride plasma sterilized; TiN-G – Titanium Nitride ETO sterilized; PU-polyurethane

Figure 2 shows the percentage of platelets and percentage of platelets aggregates circulating in blood after exposition to shear stress, presented in relation to nonactivated blood sample as the baseline.

**DISCUSSION & CONCLUSIONS:** The different Ti(N,C,O) surface layers could be successfully produced on the low profile mechanical valve ring. The chemical composition of surface layers influence on the blood contact properties, by decreasing induced platelet activation. The long term biological examination in animal experiment of POLVAD device equipped with developing valve is necessary for final validation.

**ACKNOWLEDGEMENTS:** This research was performed within the National Program of “The Polish Artificial Heart Development”

## Adhesion and growth of fibroblasts on artificial materials for tissue engineering

S. Rimpelova<sup>1</sup> N. Kasalkova<sup>2</sup> V. Svorcik<sup>2</sup> & T. Ruml<sup>1</sup>

<sup>1</sup> *Institute of Chemical Technology Prague, Department of Biochemistry and Microbiology, Technicka 5, Prague, 166 28, The Czech Republic*

<sup>2</sup> *Institute of Chemical Technology Prague, Department of Polymers, Technicka 5, Prague, 166 28, The Czech Republic*

**INTRODUCTION:** Tissue engineering (TE) is of growing importance, especially for variety of clinical applications as treatment of burns or chronic venous ulcers. Cell-material interface plays a key role in the interaction of cells with artificial materials designed for construction of body implants. Polymers have been applied for their excellent bulk properties such as low density, flexibility, strength and chemical resistance<sup>1,2</sup>. Presence of chemical functional groups on the material surface strictly influences the cell adhesion<sup>3</sup>. Plasma treatment of polymers has become an important industrial process for the modification of polymers surface used in TE<sup>3</sup>.

**METHODS:** High density polyethylene (PE) was irradiated with inert Ar plasma and the chemically active PE (0,04 mm thick foils) surface was grafted by bio-molecules of fibronectin (FN) or tripeptide RGD or glycine. The composition and the structure of the modified PE surface were studied using X-ray photoelectron spectroscopy and Rutherford backscattering spectroscopy. Changes in the surface wettability were determined from the contact angle measured in a reflection goniometer. The changes in the surface roughness and morphology were followed by atomic force microscopy. The modified PE samples were after sterilization in 96% ethanol seeded with mouse embryonal fibroblasts (NIH 3T3) with the density of 11,000 cells/cm<sup>2</sup>. The number and morphology of initially adhered cells were studied 24 h after seeding. The cell proliferation activity was achieved on the 2<sup>nd</sup>, 5<sup>th</sup> and 7<sup>th</sup> days after inoculation. Cells were fixed, stained with TRITC-Phalloidine and DAPI and evaluated by fluorescence microscope Olympus IX 81. Numbers of cells were determined by Lucia 5.20.

**RESULTS:** The plasma treatment of PE lead to increased surface roughness. Presence of new functional groups at the surface and increased wettability enabled modifying of PE by solution of bio-molecules. Number of adhered cells on plasma modified PE was bigger than on Petri's dishes. Adhesion and growth is further supported

by modification of plasmated PE by RGD and even more by FN, means, that larger proteins from ECM support more the initial cell adhesion than the minimal domain recognized by integrins – RGD. Even less attractive was modification by glycine.

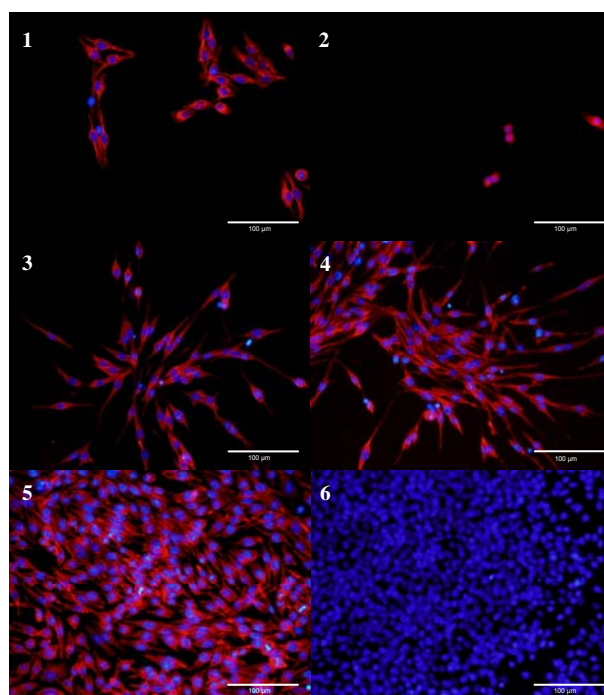


Fig. 1: NIH 3T3 growing on Petri's dish (1), pristine PE (2), plasma modified PE grafted by FN, after 24 h (3), plasma modified PE grafted with FN, 2<sup>nd</sup> day (4), 5<sup>th</sup> day (5), 7<sup>th</sup> day (6).

**DISCUSSION & CONCLUSIONS:** The positive effect of plasma treatment of PE on the adhesion and growth of NIH 3T3 was proved. Nevertheless after grafting PE by suitable biomolecules the attractiveness of PE for NIH 3T3 significantly increases. PE modified by FN supports the growth of NIH 3T3 more than its minimal sequence recognized by integrins – RGD.

**REFERENCES:** <sup>1</sup> R. Li, L. Ye, Y.W. Mai (1997) *Composites*, **28A**:73. <sup>2</sup> C.M. Chan, T.M. Ko, H. Hiroaka (1996) *Surf. Sci. Rep.* **24**:3. <sup>3</sup> Y. Choi, J. Kim, K. Paek, W. Ju, Y.S. Hwang (2005) *Surf. Coat. Technol.* **193**:319.

**ACKNOWLEDGEMENTS:** This work was supported by grants: GAAS CR KAN 200100801, VSCHT 126 08 9005, VSCHT 320 08 9033.

## Self-Inducing Geometric Cues and Bone: Formation by Autoinduction

U Ripamonti<sup>1</sup>

<sup>1</sup> *Bone Research Unit, Faculty of Health Sciences, MRC/University of the Witwatersrand, Johannesburg.*

**INTRODUCTION:** The osteogenic soluble molecular signals of the transforming growth factor- $\beta$  (TGF- $\beta$ ) superfamily, the bone morphogenetic/osteogenic proteins (BMPs/OPs) and, uniquely in the non-human primate *Papio ursinus*, the mammalian TGF- $\beta$  isoforms, induce endochondral bone formation as a recapitulation of embryonic development<sup>1</sup>. Bone tissue engineering starts by erecting scaffolds of biomimetic biomaterial matrices that mimic the supra-molecular assembly of the extracellular matrix of bone. The molecular scaffolding lies at the hearth of all tissue engineering strategies particularly *bone formation by autoinduction*<sup>2</sup>.

There is no bone formation by induction without the osteogenic soluble molecular signals of the TGF- $\beta$  super gene family. The basic tissue engineering paradigm is tissue induction and morphogenesis by combinatorial molecular protocols whereby soluble molecular signals are combined – or reconstituted – with insoluble signals or substrata acting as three-dimensional scaffolds for the initiation of *de novo* tissue induction and morphogenesis. The induction of bone formation, by combining soluble osteogenic molecular signals with different insoluble signals or substrata, is the essence of the tissue engineering paradigm. Naturally-derived highly purified and recombinant human BMPs/OPs induce bone formation in the non-human primate *Papio ursinus* and in humans, though with less efficacy as compared to animal models including non-human primates. Uniquely in the non-human primate *Papio ursinus*, the mammalian TGF- $\beta$  isoforms, the - $\beta_1$ , - $\beta_2$  and - $\beta_3$  proteins, induce substantial endochondral bone formation in heterotopic intramuscular *rectus abdominis* sites<sup>1</sup>. The insoluble signal, the carrier substratum that when combined with the osteogenic proteins triggers the bone induction cascade,<sup>1</sup> provides an exciting and novel concept of bone tissue engineering, i.e. the development of biomimetic matrices that *per se* initiate the induction of bone formation even without the addition of exogenously applied osteogenic proteins of the TGF- $\beta$  superfamily, i.e. a bioactive biomimetic matrix that *per se* differentiates resident myoblastic cells - myoendothelial cells - into osteoblastic-like cell lines expressing and secreting osteogenic gene products of the TGF- $\beta$  superfamily initiating bone

formation as a secondary response<sup>3</sup>. A solid state regulatory biomimetic matrix in which concavities differentiate myoendothelial stem cells into osteoblastic-like cells immobilizing osteogenic gene products of the TGF- $\beta$  super gene family as secreted directly onto the matrix and embedded within its regulatory concavities by differentiating osteoblastic-like cells resting within the inductive microenvironment of the concavity: the shape of life.

**RESULTS:** Our systematic studies in *Papio ursinus* have shown that the driving force of the intrinsic induction of bone formation by bioactive biomimetic matrices is the shape of the implanted scaffold; the language of shape is the language of geometry; the language of geometry is the language of a sequence of repetitive concavities that biomimetizes the remodelling cycle of the primate osteonic bone<sup>3</sup>. The remodelling cycle entails a *resting* phase with quiescent resting cells over trabeculae of bone, *activation* phase, whereby osteoclastic cells are activated to resorb mineralized bone and the *formation* phase, whereby differentiating osteoblasts appear in the lacunae and pits cut by osteoclastogenesis inducing bone formation within the concavities cut by osteoclastogenesis. The lacunae and concavities cut by osteoclastogenesis within the biomimetic matrices are the driving morphogenetic cues to induce bone formation in a *continuum* of sequential phases of resorption/ dissolution and induction of bone formation. The concavities assembled into the biomimetic matrices biomimetize the remodelling cycle of the primate cortico-cancellous bone and are endowed with multifunctional pleiotropic self-assembling capacities initiating and promoting angiogenesis and the induction of bone formation. The *connubium* of smart biomimetic matrices self-inducing gene products of the TGF- $\beta$  super gene family initiating tissue patterning, induction and morphogenesis regulated by the geometry of the substratum is the true challenge for regenerative medicine and bone tissue engineering of the 21<sup>st</sup> Century.

### REFERENCES:

<sup>1</sup>Ripamonti U (2006) *Biomaterials* **27**: 807-22

<sup>2</sup>Urist MR (1965) *Science* **150**: 893-99

<sup>3</sup>Ripamonti U (2009) *J Cell Mol Med* doi: 10.1111/j.1582.2008.00562.x

## Biomimetism, *Smart* Biomimetic Matrices and the Induction of Bone Formation

U Ripamonti<sup>1</sup> LF Renton<sup>1</sup> R Parak<sup>1</sup> L Kotze<sup>2</sup> PW Richter<sup>2</sup>

<sup>1</sup> *Bone Research Unit, Faculty of Health Sciences, MRC/University of the Witwatersrand, Johannesburg.*

<sup>2</sup> *Materials Science and Manufacturing Technology, Council for Scientific and Industrial Research, Pretoria.*

The novel concept of tissue engineering of bone is the induction of bone formation by the implantation of *smart* self-inducing biomimetic matrices endowed with shape memory geometries that *per se* initiate the ripple-like cascade of bone differentiation without the addition of exogenously applied osteogenic proteins of the transforming growth factor- $\beta$  (TGF- $\beta$ ) superfamily, the bone morphogenetic/osteogenic proteins (BMPs/OPs) and, uniquely in the non-human primate *Papio ursinus*, the three mammalian TGF- $\beta$  isoforms<sup>1,2</sup>. There is no bone formation by induction without the osteogenic soluble molecular signals of the TGF- $\beta$  super gene family. The basic tissue engineering paradigm is tissue induction and morphogenesis by combinatorial molecular protocols whereby soluble molecular signals are combined with insoluble signals or substrata acting as three-dimensional scaffolds for the initiation of *de novo* tissue induction and morphogenesis<sup>2</sup>. The induction of bone formation, by combining soluble osteogenic molecular signals with different insoluble signals or substrata, is the essence of the tissue engineering paradigm. Can we engineer biomimetic matrices that differentiate invading myoblastic myoendothelial stem cells into osteoblastic cell lines? Can we design biomimetic matrices in which differentiating osteoblast-like cells express and secrete mRNA species of the TGF- $\beta$  superfamily later embedded into the biomimetic matrix initiating bone formation as a secondary response? The molecular scaffolding lies at the hearth of all tissue engineering strategies and in particular '*bone: formation by auto induction*'<sup>3</sup>. The insoluble signal, the carrier substratum that when combined with the osteogenic proteins triggers the bone induction cascade<sup>1</sup>, provides an exciting and novel concept of bone tissue engineering, i.e. the development of biomimetic matrices that *per se* initiate the induction of bone formation even without the addition of exogenously applied osteogenic proteins of the TGF- $\beta$  superfamily, i.e. a bioactive biomimetic matrix that differentiates resident myoblastic myoendothelial cells into osteoblastic-like cell lines expressing and secreting osteogenic gene products of the TGF- $\beta$  superfamily initiating bone formation as a secondary response<sup>2,4</sup>. A solid state regulatory biomimetic matrix in which concavities *per se* differentiate myoendothelial

stem cells into osteoblastic-like cells immobilizing osteogenic gene products of the TGF- $\beta$  super gene family as secreted directly onto the matrix and embedded within the regulatory inductive micro-environment of the concavities. Our systematic studies in *Papio ursinus* have shown that the driving force of the intrinsic induction of bone formation by bioactive biomimetic matrices is the shape of the implanted scaffold; the language of shape is the language of geometry; the language of geometry is the language of a sequence of repetitive concavities that biomimetizes the remodelling cycle of the primate osteonic bone<sup>5</sup>. The remodelling cycle entails a *resting* phase with quiescent resting cells over trabeculae of bone, *activation* phase, whereby osteoclastic cells are activated to resorb mineralized bone and the *formation* phase, whereby differentiating osteoblasts appear in the lacunae and pits cut by osteoclastogenesis inducing bone formation within the concavities cut by osteoclastogenesis. The lacunae and concavities cut by osteoclastogenesis within the biomimetic matrices are the driving morphogenetic cues to induce bone formation in a *continuum* of sequential phases of resorption/dissolution and induction of bone formation which biomimetize the remodelling cycle of the primate cortico-cancellous bone<sup>4,5</sup>. The concavities assembled in highly crystalline<sup>1</sup> and/or hydroxyapatite/ $\beta$ -tricalcium phosphate biomimetic bioceramics<sup>4</sup> are endowed with multifunctional pleiotropic self-assembly capacities initiating and promoting angiogenesis and bone formation by induction by differentiating resident myoendothelial stem cells into secreting osteoblasts initiating the induction of bone formation.

### REFERENCES:

<sup>1</sup>Ripamonti U (2006). *Biomaterials* **27**:807-22

<sup>2</sup>Ripamonti U, Crooks J, Khoali L, Roden L (2009). *Biomaterials* **30**:1428-39

<sup>3</sup>Urist MR (1965) *Bone: formation by autoinduction*. *Science* **150**: 893-99

<sup>4</sup>Ripamonti U, Richter PW, Nilen RWN, Renton L (2008). *J Cell Mol Med* **12** **6B**:2609-21.

<sup>5</sup>Ripamonti U (2009). *J Cell Mol Med* doi: 10/1111/j.1582.2008.00562.x

## Novel self-assembled block copolymers for drug delivery

D Jhurry<sup>1</sup>, A Bhaw-Luximon<sup>1</sup>, V Lochee<sup>1</sup>, B Ancharaz<sup>1</sup>, A Veeren<sup>1</sup>, R Jeeta<sup>1</sup>

<sup>1</sup>Department of Chemistry, Faculty of Science, University of Mauritius, Réduit, Mauritius

**INTRODUCTION:** Nanoparticulate drug delivery systems based on amphiphilic block copolymer (ABC) micelles<sup>1,2</sup> offer various advantageous features over classical surfactant systems as drug carriers: well-defined core-shell architecture, small size (< 200 nm), relatively large surface area, high physical stability and passive targeting. Pluronics<sup>®</sup>, PEO-b-PLA or PEO-b-PCL, PEO-b-P(aminoacid) have intensively been tested for drug encapsulation and delivery. This presentation aims at giving an overview of our work on the macromolecular engineering of novel amphiphilic block copolymers via a two-pronged approach and their potential as interesting nanocarrier systems.

**RESULTS:** In a first approach, we have acted on the hydrophilic part of the ABC by substituting the PEO component with a hydrophilic polypeptide. Thus, we have successfully synthesized poly(L-lysine)-b-PCL<sup>3</sup> copolymers which self-assemble in aqueous solution into core-shell micelles in the size range 60-120 nm. Sugar molecules such as gluconolactone have also been grafted to the poly(L-lysine) block as side groups and their encapsulation efficiency compared with the previous systems. The second approach consisted of replacing the hydrophobic core of the ABC by a biodegradable polymer other than commonly studied polyesters such as PLA or PCL. Here, we reported on the synthesis of a new family of biodegradable poly(ester-ether)<sup>4</sup> and PEO-b-poly(ether-ester)<sup>5</sup> amphiphilic block copolymers.

**DISCUSSION & CONCLUSIONS:** The sizes of the poly(L-lysine)-b-PCL copolymer micelles are pH-dependent and a contraction is thus observed in PBS medium due to deprotonation of the ammonium groups and organization of the polylysine component in a coiled conformation rather than a fully extended one. Encapsulation and delivery of model drugs such as ketoprofen and ibuprofen as a function of pH has been achieved. The presence of ketoprofen in the

hydrophobic core can be thus confirmed by its UV absorbance at 260 nm. A higher loading efficiency results with the sugar-containing copolymers. In water, PEO-b-poly(ether-ester) exhibit a narrow particle size distribution with micelles having an average size of about 60 nm. Poly(dioxanone), commonly referred to as PDX, is known to undergo faster biodegradation / bioresorption than the polyesters. An interesting feature of the PEO-b-(polyester-ether) ABCs is that the biodegradability of the hydrophobic core component can now be tuned to meet the precise requirements of specific applications. Preliminary findings on drug encapsulation and *in vitro* delivery studies are quite promising. Fig 1 shows the release profile of ketoprofen from (PEO-b-PDX-co-MeDX) micelles in both PBS (pH=7.4) and water (pH=6.9) at 37°C. A similar burst effect is observed in both cases. The release rate is slightly faster in PBS than in water thereafter.

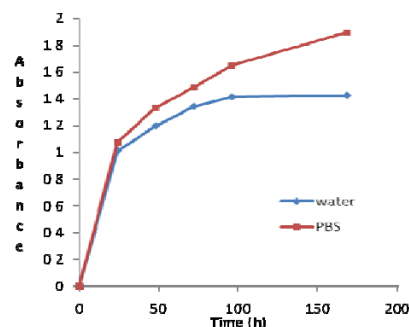


Fig. 1: Release profile of ketoprofen from (PEO-b-PDX-co-MeDX) micelles in PBS and water solutions

**REFERENCES:** <sup>1</sup> G. S. Kwon and M. L. Forrest (2006) *Drug Development Res.* **67**:15-22. <sup>2</sup> N. Nishiyama and K. Kataoka (2006) *Pharmacology and Therapeutics* **112**(3):630-48. <sup>3</sup> S. Motala-Timol, D. Jhurry, J. Zhou, A. Bhaw-Luximon, G. Mohun, H. Ritter (2008) *Macromolecules* **41**(15):5571-5576. <sup>4</sup>Y. Lochee, D. Jhurry, A. Bhaw-Luximon, A. Kalangos (under review, 2009). <sup>5</sup> Y. Lochee, A. Bhaw-Luximon, D. Jhurry, A. Kalangos (2009) *Macromolecules* **42**(19):7285-7291.

## Bone engineering around laser grooved / RGD -coated titanium surfaces.

MK Marei<sup>1</sup>, MM Saad<sup>1</sup>, RM El-Backly<sup>1</sup>, MA Alkhodary<sup>1</sup>, RA Bly<sup>2</sup>, DJ Cohen<sup>2</sup>, J Chen<sup>2</sup>, MM Fata<sup>1</sup>, WO Soboyejo<sup>2</sup>, M Nageeb<sup>1</sup>, A Rashad<sup>1</sup>, DK Ahmed<sup>1</sup>, RH Abd El-Aty<sup>1</sup>.

<sup>1</sup> *Tissue Engineering Laboratories, Faculty of Dentistry-Alexandria.* <sup>2</sup> *Mechanical and Aerospace Engineering Department, School of Engineering and applied science, Princeton University, USA.*

**INTRODUCTION:** New strategies for bone engineering e.g biomimetic surfaces including nano –or micro patterning of biomaterial surfaces or chemical modification via functionalized coating of ECM proteins or specific peptide sequences, were shown to be significant to the rational engineering of biomaterial surface and tissue response in biomedical applications .

**METHODS:** Three groups of titanium pins 5 mm length and 1.5 mm in diameter were used. The first group is the smooth pins which will be used as a control for the study, the second group is the laser grooved pins, and the third group is the laser grooved/RGD (Arginine-Glycine-Apsartic acid) coated pins. The pins were first tested in an in-vitro study, where New Zealand white rabbits bone marrow stem cells were isolated, seeded on the pins and then tested using the inverted microscope and the scanning electron microscope. This was followed by the in-vivo study, where the pins were implanted in the jaws of the rabbits for intervals of 2, 4 and 6 weeks after which the experimental animals were sacrificed, the ex-vivo samples retrieved and tested using a mechanical pull-out technique. (Figure 1)

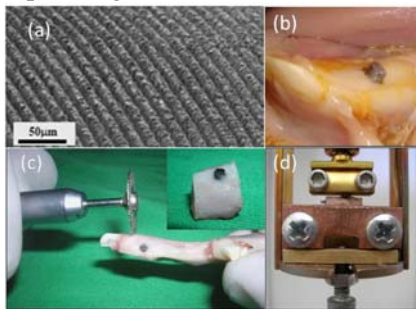


**Fig 1:** (a) Laser micro-grooved titanium surface. (b) The titanium pin implanted in the rabbit jaw. (c) Retrieving the ex-vivo sample. (d) Mechanical pull-out testing.

**RESULTS:** In the in-vitro and in-vivo studies the laser grooved/RGD coated pins had more cells attached and higher mechanical strength than the laser grooved ones, and both had improved results than the smooth surfaced pins. Histologically, the laser grooved pins have promoted new woven bone with focal adhesions spots along the surface. More adhesion was obtained with the RGD biomimetic coat, and least with control pins. (Figure2)

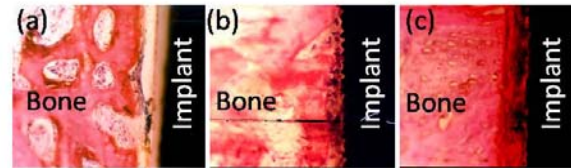


**Fig 2:** (a) Control pin, (b) the laser grooved pins.(c) laser grooved/RGD coated pin surface.

**DISCUSSION AND CONCLUSION:** In contrast to certain studies that failed to detect benefits for organic coatings, this study gave strong solid evidence on the improved micro-mechanical integration of titanium implant surfaces modified by micromachining and RGD coating.

**REFERENCES:** Schwartz J, Avaltronia M J., Danahya M P, et al (2003) Cell attachment and spreading on metal implant materials. *Materials Science and Engineering* 23: 395–400. Kroese-Deutman HC, Van Den Dolder J, et al, (2005) Influence of RGD-loaded titanium implants on bone formation *in vivo*. *Tissue Eng* 11: 1867- 75. Schliephake H, Scharnweber D, Dard M, et al, (2002) Effect of RGD peptide coating of titanium implants on periimplant bone formation in the alveolar crest. An experimental pilot study in dogs. *Clin Oral Implants Res* 13: 312-9.

**ACKNOWLEDGMENTS:** The authors deeply acknowledges the Academy of Scientific and Technological Research, Alexandria University-EGYPT, and Princeton University-USA, for their funding and support of this research work.

## Cell sheet engineering for myocardial tissue repair

T Shimizu<sup>1</sup>

<sup>1</sup> *Institute of Advanced Biomedical Engineering and Science, Tokyo Women's Medical University, TWIns, Tokyo.*

Regeneration therapy has currently emerged as one of the most promising treatments for the patients suffering from severe heart failure. Recently, bioengineered myocardial tissue transplantation has been pursued to overcome the disadvantages of isolated cell injections. We have exploited novel cell manipulation technique to construct 3-D cell-dense myocardial tissues by stacking cell sheets, which are harvested from temperature-responsive culture dishes only by lowering temperature. Stacked rat cardiomyocyte sheets simultaneously beat in macroscopic view and survived in vivo up to above 1-year. Myoblast sheets and mesenchymal stem cell sheets originated adipose tissue as well as cardiomyocyte sheets improved damaged heart function. Furthermore, endothelial co-culture promoted neovascularization and accelerated the effect of cell sheet transplantation. Recently autologous myoblast sheet transplantation has been clinically applied. As next step, we have challenged to introduce blood vessels within bioengineered myocardial tissues for overcoming size-limitation. Multi-step transplantation of triple-layer cell sheets was performed and finally, 10-time transplantations have realized about 1 mm-thick functional myocardial tissue. Furthermore, we have fabricated functional myocardial tubes by wrapping cell sheets. Bioengineered myocardial tubes can evoke the inner pressure both in vitro and in vivo. Cell sheet engineering should have enormous potential in myocardial tissue regeneration.

### REFERENCES

Shimizu T, Sekine H, Yamato M, Okano T. *Curr Pharm Des.* 2009;15:2807-14. Sekine H, Shimizu T, Hobo K, Sekiya S, Yang J, Yamato M, Kurosawa H, Kobayashi E, Okano T. *Circulation.* 2008;118:S145-52. Sekine H, Shimizu T, Yang J, Kobayashi E, Okano T. *Circulation.* 2006;114:I87-93. Shimizu T, Sekine H, Yang J, Isoi Y, Yamato M, Kikuchi A, Kobayashi E, Okano T. *FASEB J.* 2006;20:708-10. Shimizu T, Yamato M, Kikuchi A, Okano T. 2003;24:2309-16. Shimizu T, Yamato M, Isoi Y, Akutsu T, Setomaru T, Abe K, Kikuchi A, Umezumi M, Okano T. *Circ Res.* 2002;90:e40-48.

## Designer Self-assembling Peptide Biological Materials

[S Zhang](#)<sup>1</sup>

<sup>1</sup> *Center for Biomedical Engineering NE47-379, Center for Bits & Atoms Massachusetts Institute of Technology Cambridge, Massachusetts*

Short peptides that are made of natural amino acids were never seriously considered as useful materials as recent as 16 years ago. However, the discovery of a class of self-assembling peptides that spontaneously undergo self-organization into well-ordered structures resulted in a conceptual change. Since then diverse classes of short peptides have been invented with broad applications including 3D tissue cell culture, reparative and regenerative medicine, tissue engineering, slow drug release, stabilization of membrane proteins for develop nanobiotechnology and molecular devices. Molecular design using short peptides as new materials may play increasingly important role in nanoscience, nanotechnology, nanobiotechnology and nanomedicine.

Shuguang Zhang's laboratory focuses on developing new classes of biological materials using natural amino acids through molecular self-assembly. He employs the 'bottom-up' approach to produce new materials, molecule by molecule for novel supramolecular architectures. Such approach requires a deep understanding of individual molecular building blocks, their structures, assembling properties and dynamic behaviors. Two key elements in molecular fabrication are chemical complementarity and structural compatibility, both of which confer the weak and noncovalent interactions that bind building blocks together during molecular self-assembly. Significant advances have been achieved at the interface of biology, chemistry and materials science including: 1) the fabrication of nanofiber scaffolds for 3-D cell cultures, tissue repair and regenerative medicine, 2) the designer peptide surfactants for stabilizing and crystallizing membrane proteins Molecular fabrications of biological materials accelerate diverse scientific discoveries and technological innovations.

### REFERENCES:

Zhao, X. & Zhang, S. (2006) *Royal Society of Chemistry* **35**, 1105-1110. Zhang, S. (2007). *Advances in Cancer Research* **99**, 335-362. Horii, A., Wang, X & Zhang, S. (2008) In *Nanotechnology & Tissue Engineering: The*

*Scaffold*. (Ed. Nair, L.S.). Taylor & Francis Publishing, New York, pp.283-292. Yang, Y. Khoe, U., Wang, X., Horii, A., Yokoi, H., & Zhang, S., (2009) *Nano Today* **4**, 193-210.

## Synthesis of Bio-Based Polyester From Sorghum- Derived 1, 3-Propanediol.

C M Obele<sup>1</sup> & O. Ogbobe<sup>2</sup>

Department of *Polymer and Textiles Engineering*, Nnamdi Azikiwe University, Awka, Nigeria<sup>2</sup> Department Of Polymer and Textile Engineering, Federal University of Technology Owerri, Nigeria

**INTRODUCTION:** A bio- based polyester (polytrimethylene phthalate) has been synthesized using a sorghum derived 1, 3 – propanediol and phthalic acid, the diol employed in the synthesis was obtained biologically by converting sorghum starch to sugar using a dual enzyme technique. The reaction lasted 3hrs. 05mins. The reaction temperature was  $120^{\circ} \pm 5^{\circ}\text{C}$ . A white semi-crystalline solid which will find applications in fiber production, carpet backings, medicine and coatings was obtained.

**METHODS:** The polyester was characterized using infrared spectroscopy and thermal analysis.

**RESULTS:** The infrared spectrum and the thermogram are shown in figures 1, &2, Table 1 below shows the most important absorption in the infrared spectrum and the corresponding assignments. From the DTA graph, the melting point of the polyester was  $222.6^{\circ}\text{C}$  while the TG is  $65.94^{\circ}\text{C}$ .

Table1: Most important absorption and corresponding assignments.

Wave number (cm <sup>-1</sup> )	Assignment, Moiety
3330	Carboxylic acid
2800 - 3000	C-H – Alkyl group
1450 - 1600	C – C – Aryl
1100 – 1300	C – O - Esters

**DISSCUSSION & CONCLUSIONS:** The thermogravimetric analysis (TGA) results revealed that degradation took place in two stages. The major weight loss was 2.75mg of the sample corresponding to 24.34%. This showed that the polyester had high stability. The results obtained from the i.r. indicated that the material synthesized was the polyester – poly (trimethylene phthalate).

### REFERENCES:

<sup>1</sup>J. Ross, D. Tian and G. Sigel (2008). *Polyester fiber compositions*. W0/2008/042384. <sup>2</sup> X.yong,

Hong–Bing, Y. Sheng–Rong and H. Jian (2007). *J. of Matter Sci.* 42, 19 p.8381 -8385. <sup>3</sup> Allen et al (2003). *Zero Heel Polyester Process*. US Pat. NO 6528579. <sup>4</sup> K. Chrissafis, K.M Paraskevopoulos and D.N Bikiaris (2006). *Thermochimica Acta* 44, 175.

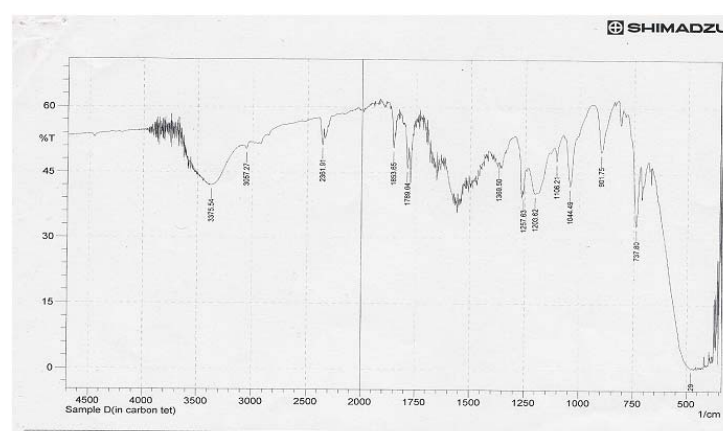


Fig.1: Fourier transform infrared spectrum of Poly (trimethylene Phthalate).

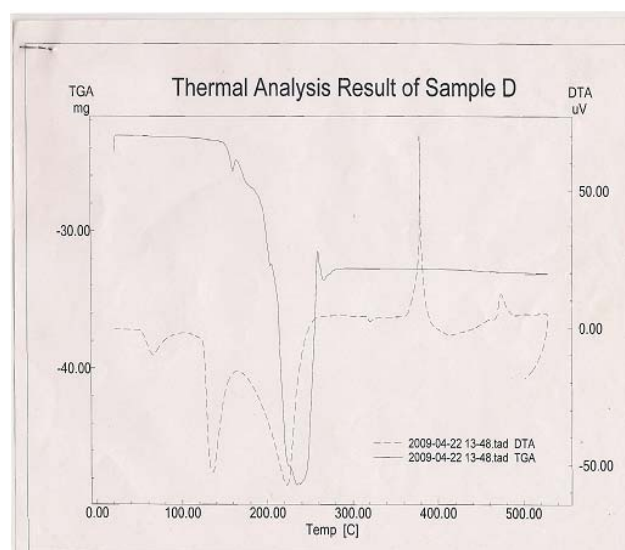


Fig. 2: Thermal Analysis curves from Poly (trimethylene phthalate).